

Spatially-explicit correction of simulated urban air temperatures using crowd-sourced data

Oscar Brousse^{1,1}, Charles H. Simpson^{1,1}, Owain Kenway^{1,1}, Alberto Martilli^{2,2}, Scott Krayenhoff^{3,3}, Andrea Zonato^{4,4}, and Clare Heaviside^{1,1}

¹University College London

²CIEMAT

³University of Guelph

⁴Atmospheric Physics Group, Department of Civil, Environmental and Mechanical Engineering, University of Trento, Trento, Italy

May 22, 2023

Abstract

Urban climate model evaluation often remains limited by a lack of trusted urban weather observations. The increasing density of personal weather stations (PWS) make them a potential rich source of data for urban climate studies that address the lack of representative urban weather observations. In our study, we demonstrate that PWS data not only improve urban climate models' evaluation, but can also serve for bias-correcting their output prior to any urban climate impact studies. After simulating near-surface air temperatures over London and south-east England during the hot summer of 2018 with the Weather Research Forecast (WRF) model and its Building Effect Parameterization with the Building Energy Model (BEP-BEM) activated, we evaluated the modelled temperatures against 402 urban PWS and showcased a heterogeneous spatial distribution of the model's cool bias that was not captured using official weather stations only. This finding indicated a need for spatially-explicit urban bias corrections of air temperatures, which we performed using an innovative method using machine learning to predict the models' biases in each urban grid cell. Our technique is the first to consider that urban temperatures are heterogeneously accurate in space and that this accuracy is not linearly correlated to the urban fraction. Our results showed that the bias-correction was beneficial to bias-correct daily-minimum, -mean, and -maximum temperatures in the cities. We recommend that urban climate modellers further investigate the use of PWS for model evaluation and derive a framework for bias-correction of urban climate simulations that can serve urban climate impact studies.

1 **Spatially-explicit correction of simulated urban air temperatures using**
2 **crowd-sourced data**

3 Oscar Brousse,^a Charles Simpson,^a Owain Kenway,^b Alberto Martilli,^c E. Scott Krayenhoff,^d
4 Andrea Zonato,^e and Clare Heaviside,^a

5 ^a*Institute of Environmental Design and Engineering, University College London*

6 ^b*Centre for Advanced Research Computing, University College London*

7 ^c*Center for Energy, Environment and Technology (CIEMAT)*

8 ^d*School of Environmental Sciences, University of Guelph*

9 ^e*Department of Civil, Environmental and Mechanical Engineering, University of Trento*

10 *Corresponding author: O. Brousse, o.brousse@ucl.ac.uk*

11 **ABSTRACT:** Urban climate model evaluation often remains limited by a lack of trusted urban
12 weather observations. The increasing density of personal weather stations (PWS) make them
13 a potential rich source of data for urban climate studies that address the lack of representative
14 urban weather observations. In our study, we demonstrate that PWS data not only improve urban
15 climate models' evaluation, but can also serve for bias-correcting their output prior to any urban
16 climate impact studies. After simulating near-surface air temperatures over London and south-
17 east England during the hot summer of 2018 with the Weather Research Forecast (WRF) model
18 and its Building Effect Parameterization with the Building Energy Model (BEP-BEM) activated,
19 we evaluated the modelled temperatures against 402 urban PWS and showcased a heterogeneous
20 spatial distribution of the model's cool bias that was not captured using official weather stations
21 only. This finding indicated a need for spatially-explicit urban bias corrections of air temperatures,
22 which we performed using an innovative method using machine learning to predict the models'
23 biases in each urban grid cell. Our technique is the first to consider that urban temperatures are
24 heterogeneously accurate in space and that this accuracy is not linearly correlated to the urban
25 fraction. Our results showed that the bias-correction was beneficial to bias-correct daily-minimum,
26 -mean, and -maximum temperatures in the cities. We recommend that urban climate modellers
27 further investigate the use of PWS for model evaluation and derive a framework for bias-correction
28 of urban climate simulations that can serve urban climate impact studies.

29 SIGNIFICANCE STATEMENT: Urban climate simulations are subject to spatially heteroge-
30 neous biases in urban air temperatures. Common validation methods using official weather stations
31 do not suffice for detecting these biases. Using a dense set of personal weather stations in London
32 we detect these biases before proposing an innovative way for correcting them with machine learn-
33 ing techniques. We argue that any urban climate impact study should use such technique if possible
34 and that urban climate scientists should continue investigating paths to improve our methods.

35 **1. Introduction**

36 Although decades following the 1960s have seen an increase in the body of literature on urban
37 climates (Oke et al. 2017), the scales of applicability and the transferability of their outcomes are
38 often limited. This can partially be attributed to the lack of observations representative of the
39 variety of existing urban climates in cities. To address this limitation, two major solutions were
40 proposed over the past 20 years: firstly, the development of urban surface energy balance coupled
41 to regional climate models (e.g., Masson (2000), Martilli et al. (2002), Wouters et al. (2016)),
42 and secondly, the increased interest towards crowd-sourced and low-cost weather sensors (e.g.,
43 Muller et al. (2015), Chapman et al. (2017), Fenner et al. (2017), Meier et al. (2017)). After
44 proper validation and parameterization, urban climate models (UCMs) offer an unprecedented
45 opportunity to represent the impact of cities on a wide variety of weather variables at very high
46 spatial and temporal resolutions. This has been further supported by the recent development of
47 global standardized land use land cover datasets designed for urban climate studies that permit
48 their parameterization in cities formerly deprived of these data (see the World Urban Dataset and
49 Access Portal Tool (WUDAPT) project; Ching et al. (2018), Demuzere et al. (2022)). Likewise,
50 after proper filtering and quality control (Napoly et al. 2018; Fenner et al. 2021), crowd-sourced
51 personal weather sensors (PWS) permit the extension of sensing networks into urban environments
52 that were formerly not studied despite the fact that PWS often do not meet the standards imposed
53 by official meteorological offices for implementation of weather stations. Several studies have
54 demonstrated their range of applications since then (e.g., Fenner et al. (2019), Venter et al. (2020),
55 Potgieter et al. (2021), Benjamin et al. (2021), Varentsov et al. (2021), Venter et al. (2021), Brousse
56 et al. (2022)).

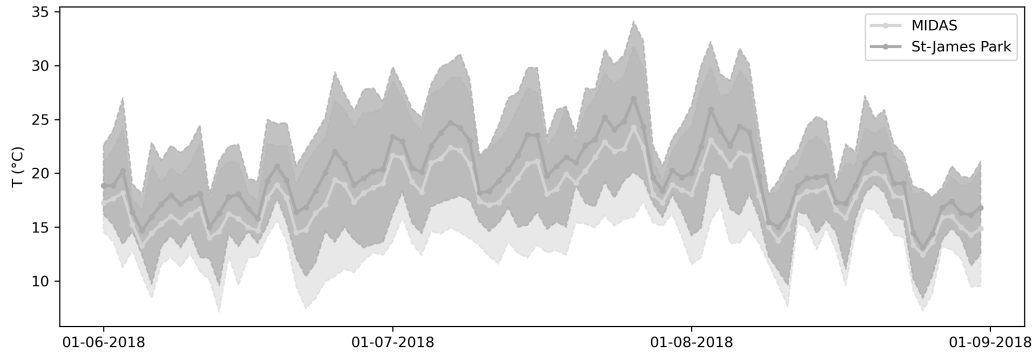
57 One of the major limitations induced by the lack of official weather stations in cities is that
58 quantifying existing uncertainties as a function of urban climate archetype is not feasible. This
59 means that certain urban environments are poorly evaluated and hence modelled, assuming that
60 UCMs will perform similarly under all constraints imposed by the variety of urban environments
61 that compose a city. In face of this challenge, crowd-sourced PWS could improve the evaluation
62 of UCMs, as Hammerberg et al. (2018) demonstrated over Vienna. But the potential of PWS may
63 even be greater, particularly when used jointly with or in parallel to UCMs. In fact, a recent study
64 by Sgoff et al. (2022) improved the weather forecasting of the Icosahedral Nonhydrostatic Model
65 (ICON; Zängl et al. (2015)) at a horizontal resolution of 2 km over Germany by assimilating the
66 data provided by PWS for air temperature and relative humidity at 2 m height. Although data
67 assimilation occurs at runtime, PWS could also be used to bias-correct urban climate simulations
68 as a post-processing step. Oleson et al. (2018) already noted the need for a global dataset of
69 urban weather observations to properly bias-correct simulated urban climates. We indeed expect
70 urban climate simulations to have systematic biases that can be induced for a variety of reasons,
71 such as: urban canopy parameters (Demuzere et al. 2017; Hammerberg et al. 2018; Zonato et al.
72 2020); complexity of urban climate models (Grimmond et al. 2011; Loridan and Grimmond 2012;
73 Lipson et al. 2021); time at which the simulation is initialised (Bassett et al. 2020); choice of initial
74 and boundary conditions for lateral and vertical forcing (Brisson et al. 2015); or choice of model
75 parameterizations – such as the two evaluated in this work (see Methods). Hence, UCM will always
76 present a certain degree of uncertainty that has to be allowed for prior to performing urban climate
77 impact studies that use climatic variables derived from modelled simulations to estimate the impact
78 of the urban climate on other things (e.g. mortality, biodiversity, etc.). Using PWS could thus be
79 beneficial for obtaining realistic urban weather data of present and future urban climates that can
80 be used to perform urban climate impact studies and guide decision-making.

81 In this study, we propose to leverage the increasingly dense network of PWS over south-east
82 England since 2015 (Brousse et al. 2022) to evaluate and bias-correct urban climate simulations
83 that were run for the hot summer of 2018 – the hottest summer on average in the UK. Common
84 practices in bias-correction include adding the mean bias to the modelled variable distribution or
85 applying a separate correction to each quantile of the distribution (Maraun and Widmann 2018).
86 Model biases are usually measured at official weather stations at rural sites, thereby assuming

87 that the urban heat island phenomenon is accurately represented by the UCM (e.g., Lauwaet et al.
88 (2015), or Oleson et al. (2018)). Some studies however tried considering the urban effect by linearly
89 transforming the bias-correction coefficient via an urbanization ratio calculated at each grid cell,
90 like in Wouters et al. (2017) over Belgium. Assuming that urban climate simulations biases cannot
91 be linearly related to the urban fraction only, we decided to test whether urban in-situ observations
92 can be used to perform an urban-specific bias-correction of air temperatures driven by machine
93 learning.

94 We chose to use machine learning regressors to correct the air temperature biases because machine
95 learning allows us to perform spatially explicit bias-corrections that are directly derived from the
96 observed biases at all PWS locations and that are related to a set of spatially explicit covariates.
97 Machine learning regressors of ranging complexities allow for the statistical discretisation of a
98 single relationship between the covariates and the variety of biases. To our knowledge, such
99 a technique has never been proposed as a viable approach for bias-correction of urban climate
100 simulations, probably because of the lack of observations in urban areas. We hereby hypothesize
101 that such an innovative bias-correction method would be beneficial for urban heat impact studies
102 by improving the UCM outputs on which they rely. Such innovations are needed to better assess
103 the heat burden in cities (Nazarian et al. 2022).

104 To respond to these issues through the scope of urban near-surface temperatures, we: i) evaluated
105 the ability of the complex three-dimensional UCM embedded in WRF – the Building Effect
106 Parameterization coupled with its Building Energy Model (BEP-BEM) – to accurately represent
107 the urban impact on air temperatures under two boundary layer schemes for the summer of 2018 in
108 south-east England using official weather stations and PWS separately to show their added value for
109 detecting spatially heterogeneous urban temperature biases; ii) used machine learning regressions
110 to predict the models' daily air temperature biases in the urban environment and bias-correct the
111 two simulations suggested in part i – which allowed us to determine an optimal time-step at which
112 the bias-correction should be performed to optimize the outputs.; and iii) compared the two bias-
113 corrected products against the predicted daily air temperatures using only PWS measurements to
114 investigate how realistic the bias-corrected products are. In parallel, to illustrate the benefit gained
115 from the bias-correction for impact studies, we showcase how the bias-correction leads to different
116 population weighted temperatures in the Greater London area. We also estimated the amount of



131 FIG. 1. Diurnal ranges of temperatures observed by the Met Office MIDAS automatic weather stations. The
 132 urban St-James' Park station in central London (dark grey) is always hotter than the average temperature of all
 133 MIDAS stations in south-east England (light grey) for daily average, minimum and maximum temperatures. The
 134 thick lines represent the daily average temperature and the shading represent the spread between daily maxima
 135 and minima.

117 PWS that are necessary to achieve optimal machine learning regressors performance and tested the
 118 added value of official weather stations for bias-correction.

119 It is important to consider that our study does not try to estimate how a bias-corrected modelled
 120 product is better compared to a predicted product from observations for urban climate impact
 121 studies. We hereby simply try to demonstrate that any urban climate impact work that is based on
 122 urban climate modelling should pursue a spatially explicit bias-correction specific to urban areas.

123 2. Methods

124 a. Model setup and region of interest

125 We focused our study on the south-eastern parts of England, centred over the metropolis of
 126 London, host to approximately 9 million inhabitants. We chose to model the impact of urbanization
 127 on 2 m air temperature in London during the summer of 2018, since it was the hottest summer on
 128 average in the UK (McCarthy et al. 2019). During the the British Isles heatwaves, maximum daily
 129 temperatures often surpassed 30 °C (Figure 2)with a maximum of 34.4 °C measured at London's
 130 Heathrow airport on the 26th of July. This former record has yet been broken in 2019 and 2022.

136 To model the impact of the urban areas of London and south-east England on local meteorology,
137 we used the Weather Research Forecast (WRF) regional climate model version 4.3 and activated
138 the embedded Building Effect Parameterization (BEP; Martilli et al. (2002)) urban climate model
139 with its partner Building Energy Model (BEM; Salamanca et al. (2010); Salamanca and Martilli
140 (2010)) – hereafter referred to as BEP-BEM. We ran the model at a horizontal resolution of 1 x
141 1 km following a two-way nesting strategy where the outer domain is forced by ERA5 6-hourly
142 data at 25 km with 199 by 199 grid points and the two intermediate domains are run at horizontal
143 resolutions of 9 and 3 kilometres with 252 by 241 and 210 by 180 grid points, respectively (Figure 2,
144 upper panel). Initial land surface conditions were provided by the default MODIS 5-arc-second
145 land use dataset provided by the WRF community while sea surface temperatures were updated
146 6-hourly out of ERA-5. No lake models were activated, hence meaning that inland fresh water
147 bodies are given the MODIS Water land cover class and are not updated on 6-hourly time steps as
148 sea-surface temperatures. We ran the model in parallel over 200 CPUs using restarts every four
149 days of simulation. We started the simulations on the 25th of May 2018 and end them on the 31st
150 of August 2018, considering the first 7 days of simulation as spin-up time.

151 All domains used the same physical and dynamical parameterizations which we obtained out of
152 preliminary testing done over the two hottest days of the summer 2018 – 26th and 27th of July 2018
153 (see Appendix A). We thereby used the WRF Single-moment 3-class microphysics scheme (Hong
154 et al. 2004), the Dudhia shortwave and RRTM longwave schemes (Dudhia 1989; Mlawer et al.
155 1997), and the revised MM5 surface layer scheme (Jiménez et al. 2012). In the first domain, the
156 Kain-Fritsch convection scheme was activated (Kain 2004) and then turned off in the second and
157 third domains, which were at convection-permitting scales. We set the model top at 50 hPa with an
158 additional 5000 m damping layer and subdivided the atmosphere into 56 vertical layers. We used
159 the Noah-MP land surface scheme (Niu et al. 2011; Yang et al. 2011) in its default parameterization
160 over 4 soil layers.

163 Urban canopy parameters required by the WRF BEP-BEM model were provided via the newly
164 standardized WUDAPT-TO-WRF (W2W) python package developed by Demuzere et al. (2021),
165 following the Fortran version used by Brousse et al. (2016). This allowed the transfer of spatially-
166 explicit morphological urban canopy parameters suitable for urban climate simulations via Local
167 Climate Zones (LCZ) maps covering the inner domain (Figure 2, lower panel). We use the

161 **Table 1.** Thermal and radiative parameters per LCZ based on Stewart et al. (2014). Road parameters are considering a mixture of asphalted and
162 concrete road pavements and grass.

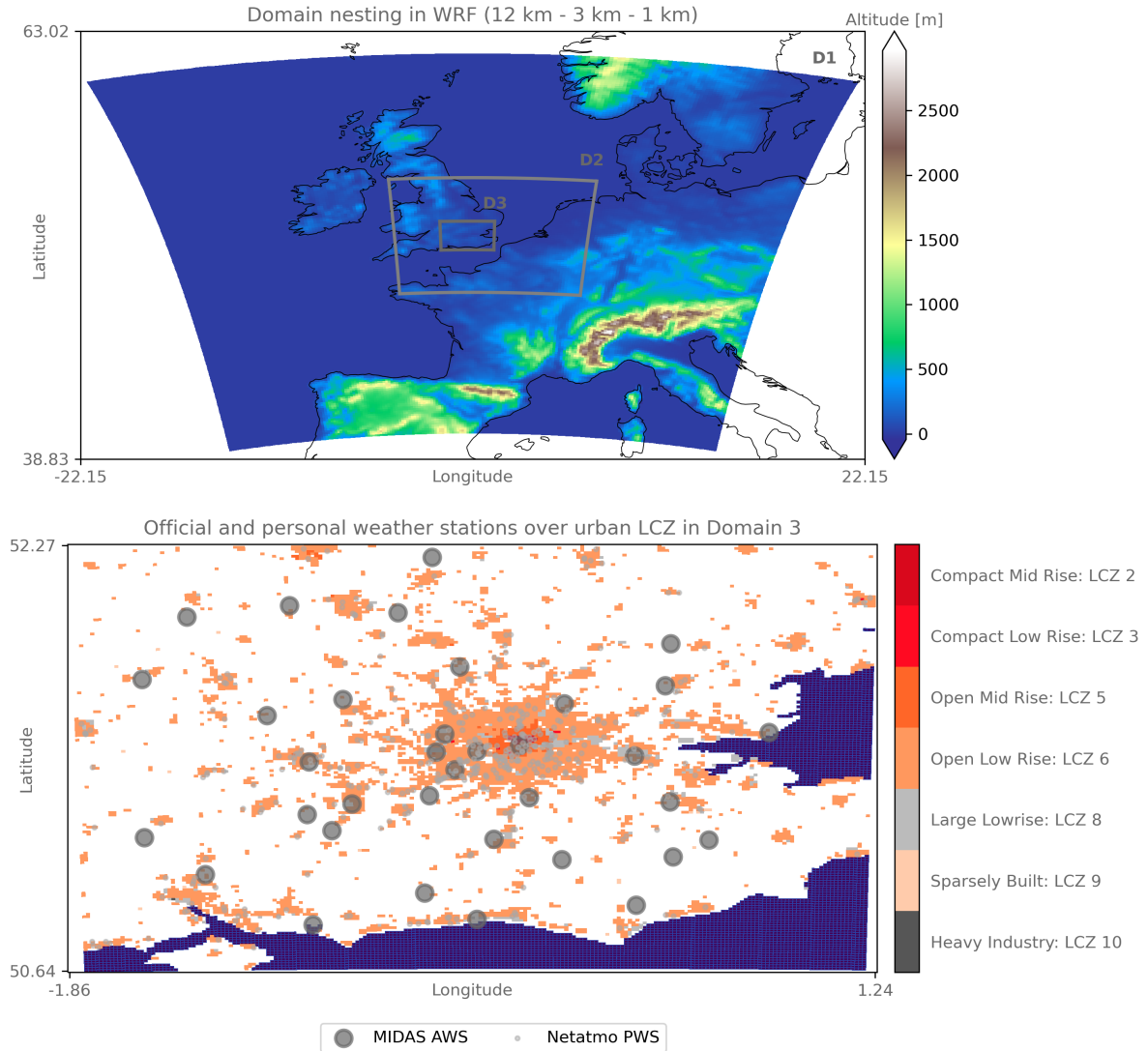
	Heat capacity			Thermal conductivity			Albedo			Emissivity		
	Roof	Wall	Road	Roof	Wall	Road	Roof	Wall	Road	Roof	Wall	Road
	[$J \cdot m^{-3} \cdot K^{-1}$]			[$J \cdot m^{-1} \cdot s^{-1} \cdot K^{-1}$]								
LCZ 1	1.80E+06	1.80E+06	1.75E+06	1.25	1.09	0.77	0.13	0.25	0.15	0.91	0.90	0.95
LCZ 2	1.80E+06	2.67E+06	1.65E+06	1.25	1.50	0.73	0.18	0.20	0.16	0.91	0.90	0.95
LCZ 3	1.44E+06	2.05E+06	1.63E+06	1.00	1.25	0.69	0.15	0.20	0.18	0.91	0.90	0.95
LCZ 4	1.80E+06	2.00E+06	1.54E+06	1.25	1.45	0.60	0.13	0.20	0.20	0.91	0.90	0.95
LCZ 5	1.80E+06	2.00E+06	1.50E+06	1.25	1.45	0.62	0.13	0.25	0.20	0.91	0.90	0.95
LCZ 6	1.44E+06	2.05E+06	1.47E+06	1.00	1.25	0.60	0.13	0.25	0.21	0.91	0.90	0.95
LCZ 7	2.00E+06	7.20E+05	1.38E+06	2.00	0.50	0.51	0.15	0.20	0.24	0.28	0.90	0.92
LCZ 8	1.80E+06	1.80E+06	1.80E+06	1.25	1.25	0.80	0.18	0.25	0.17	0.91	0.90	0.95
LCZ 9	1.44E+06	2.56E+06	1.37E+06	1.00	1.00	0.55	0.13	0.25	0.23	0.91	0.90	0.95
LCZ 10	2.00E+06	1.69E+06	1.49E+06	2.00	1.33	0.61	0.10	0.20	0.21	0.91	0.90	0.95

168 European LCZ map by Demuzere et al. (2019). Thermal and radiative parameters are also directly
169 derived from the LCZ classification and follow those used by Stewart et al. (2014), who used these
170 parameters for the city of Basel, Switzerland. Each parameter for roofs, walls and roads is related to
171 each modal LCZ of the 1 km grid cell via the `URBPARAM_LCZ.TBL` (see Table 1). We decided to
172 keep the roughness length for momentum and the lower boundary for temperatures of roofs, walls,
173 and roads identical across each LCZ. We fixed the roughness length at $1.00E-4$ m for walls and at
174 0.01 m for roofs and roads, respectively. This does not mean that the effective roughness length at
175 the bulk level does not differ between urban morphologies. Although materials composing them
176 are considered identical in the drag they impose on the flow, their density and height will matter.
177 Urban canyons with buildings above 25 m and another with buildings below 5 m will effectively
178 have a different roughness length. For the boundary temperatures, we set it at 299 K for the roofs
179 and the walls, respectively, and at 293 K for the road. We chose to deactivate the air conditioning
180 in our simulation because air conditioning systems are not common in residential areas across
181 London and surrounding cities, which compose the major part of the land use land cover.

189 In this study, two potential planetary boundary layers (PBL) schemes are compared in terms
190 of performance and need of bias correction: the commonly used Bougeault-Lacarrère scheme
191 (BouLac; Bougeault and Lacarrere (1989)) for urban simulations that use BEP-BEM, and the
192 recently coupled YSU scheme to BEP-BEM (Hong et al. 2006; Hong and Kim 2008; Hendricks
193 et al. 2020). Although we found that the latter performed better over the two hottest days of
194 summer 2018 (see Appendix A), we decided to keep a simulation with BouLac as YSU has only
195 been applied over Dallas (Wang and Hu 2021) whereas BouLac has been used in multiple studies
196 already (e.g., Salamanca et al. (2011), Salamanca et al. (2012), Gutiérrez et al. (2015), Tewari
197 et al. (2017), Mughal et al. (2019)). The Mellor-Yamada-Janjic (MYJ; Janjić (1994), Janić (2001))
198 scheme, also available for BEP-BEM simulations, is disregarded in this study since this PBL
199 scheme is especially used for mountainous terrain (Zonato et al. 2022), and we are modelling the
200 relatively flat terrain of south-east England.

201 *b. Model evaluation prior to bias correction*

202 We evaluated the model's performances against 35 official weather stations' measurements of
203 air temperature at 2 m obtained from the UK Met Office MIDAS network (Sunter (2021), UKMO



182 FIG. 2. Domain nesting (upper) and urban land cover in the inner domain (lower). The WRF nesting strategy
 183 consists of three nested domains at 12 km (D1), 3 km (D2) and 1 km (D3) horizontal resolution. The altitude is
 184 plotted to highlight the flat terrain of south-east England covered in D3. In the lower panel, the resulting urban
 185 landcover in D3 after using the WUDAPT-TO-WRF python tool is presented in the form of Local Climate Zones
 186 (LCZ). The MIDAS official automatic weather stations (AWS) and the Netatmo personal weather stations (PWS)
 187 used for the evaluation of the model and the subsequent bias-correction using PWS only are overlaid in grey.
 188 The sea is shown in blue in the lower panel while coastlines are drawn in black in the upper panel.

204 (2021); Figure 1, lower panel). To address the issue of lack of official observations amongst the
205 urban environment, we used Netatmo PWS to complement the model evaluation (Figure 1, lower
206 panel). The Netatmo PWS measurements were obtained through the Netatmo App developer API
207 and were collected for all PWS contained within the inner most domain of WRF and that were
208 running over the 2015 to 2020 period (more information can be found in (Brousse et al. 2022)).
209 Prior to the evaluation, unrealistic PWS measurements were filtered out using the Crowd-QC v1.0
210 R package from Grassmann et al. (2018). This statistical quality check and filtering method is
211 based on the assumption that the whole set of PWS should be regarded as a reference to individual
212 stations specificities. Through four main obligatory quality-checks – potentially complemented
213 by three optional – erroneous data are removed. Details of this filtering method can be found in
214 other publications like Napoly et al. (2018) and or Brousse et al. (2022) who used the same dataset
215 over London. For the summer 2018, the filtering reduced the dataset from 935 potential PWS to
216 909 potential stations over the whole domain. Such filtering has already been applied over several
217 studies, including a large scale study by Venter et al. (2021) over a European city, and has recently
218 been ameliorated into the *CrowdQC+* package (Fenner et al. 2021). The purpose of this study is
219 not to test the effect of PWS quality check on the model evaluation and bias correction.

220 After quality-checking the PWS we also added an additional filtering where we removed PWS
221 that did not have sufficient temporal data coverage and that were not located in an urban pixel
222 according to WRF. Only PWS that have less than 4 hours per day without data and that are
223 located in urban pixels with an urban fraction greater than 0 are retained – where the WRF
224 land-use land-cover at 1 km horizontal resolution refers to an LCZ. This ensures that we do not
225 include measurements that are not representative of the daily variations in air temperatures or
226 built-up environments. Additionally, the prior filtering performed using the *CrowdQC* package
227 also ensures that measurements that are not representative of outdoor thermal variations (e.g.,
228 indoor sensors) or that are resulting from defective sensors are taken out. Overall, the filtering
229 step is necessary to ensure that our model outputs are evaluated against measurements of sufficient
230 quality and that the subsequent bias-correction is deprived of unnecessary noise in the data that
231 could lower its performance. This resulted in a sample of 402 PWS usable for model evaluation
232 and bias correction. Out of these, 354 were located in WRF grids classified as LCZ 6, 30 in LCZ 5,
233 8 in LCZ 2, 6 in LCZ 8, 3 in LCZ 9 and 1 in LCZ 3.

234 Each model simulation was evaluated using a set of common statistical indicators: the root mean
235 squared error (RMSE), the mean absolute error (MAE), the mean bias error (MB), Spearman’s
236 coefficient of correlation (r) and the square of Pearson’s coefficient of correlation (r^2). These
237 metrics are obtained using the Python scikit-learn and scipy’s stats packages from Pedregosa et al.
238 (2011) and Virtanen et al. (2020).

239 *c. Bias correction using personal Netatmo weather stations*

240 In our study, we propose an innovative method to bias-correct urban temperatures at a horizontal
241 scale of 1 km by using machine learning regression. The advantage of using machine learning
242 regression compared to more common bias-correction strategies (e.g., the definition of a single
243 bias coefficient) is that we are able to relate our model output biases out of spatially varying and
244 explicit sets of parameters. In our case, we make the assumption that the spatial variation in the
245 bias of the model is dependent only upon the spatial morphological inputs to the UCM. These
246 include the urban fraction, the surface height, the average building height, the building surface to
247 plan area fraction (λ_b), the plan area fraction (λ_p) and the frontal area fraction (λ_f). Using this set
248 of predictive covariates, we train our regressors to predict the bias in the modelled air temperature
249 at 2 m (T_2) based on observed biases at urban PWS locations. This way, we are able to bias-correct
250 the modelled temperatures in each urban pixel based on the predicted bias ($T_2 - \text{bias}_{pred}$). Our
251 bias-correction does not make use of official MIDAS weather stations as their use is considered
252 detrimental to the bias correction following an analysis on sample size and sensor types given in
253 Appendix B.

254 We chose to bias-correct the simulated daily minimum, maximum and average T_2 (T_{2min} , T_{2max} ,
255 and T_{2mean}) using filtered PWS observations in London and south-east England. Daily temporal
256 scale is considered optimal as it combines a higher spatial density of measurements compared to
257 hourly data and a lower computational requirement; it is also a commonly used temporal scale
258 for urban heat impact studies. Daily minimum and maximum air temperatures at 2 m are defined
259 following the Met Office Had-UK definition: minimum temperature observed from 9AM of the
260 previous day $d-1$ to 9AM of the d day, and maximum temperature observed from 9AM of the d
261 day to 9AM of the next day $d+1$ (Hollis et al. 2019).

TABLE 2. Hyperparameter tuning used by each regressors

Model	Parameters Dictionary
Linear	'normalize': False
Ridge	'alpha': 1, 'normalize': True, 'random_state': 42, 'solver': 'lsqr', 'tol': 0.01
Lasso	'alpha': 1, 'normalize': False, 'random_state': 42, 'selection': 'random', 'tol': 1e-10
Random Forest	'max_features': 'sqrt', 'min_samples_leaf': 11, 'min_samples_split': 2, 'n_estimators': 400, 'random_state': 42
Gradient Boosting	'learning_rate': 0.2, 'max_depth': 3, 'max_features': 'sqrt', 'min_samples_leaf': 10, 'min_samples_split': 22, 'n_estimators': 200, 'random_state': 42, 'subsample': 0.2

262 We test the ability of 6 different regressors of increasing complexity available in the Python scikit-
263 learn packages (Pedregosa et al. 2011) to predict the model bias based on WRF spatial urban canopy
264 parameters only. These regressors are: dummy regression (which simply returns the mean bias),
265 linear regression, Ridge regression, Lasso regression, Random Forest regression, and Gradient
266 Boosting regression. Each of the different regressors, except the dummy regression, offers a set of
267 parameters that can be fine-tuned to increase each regressor's performance. Hence, prior to running
268 the daily bias-correction we use a 5 K-fold cross-validation using the *Grid Search CV* package
269 from scikit-learn in Python to evaluate the impact of hyperparameter tuning on the regressors'
270 performances based on RMSE, MAE and r^2 . The cross-validation is done over the summertime
271 average daily mean temperature bias from the YSU run only, for computational reasons. We retain
272 RMSE as the refitting score to better capture the spatial spread and extremes of T2. The resulting
273 parameterizations are given in Table2. We chose to keep the same hyperparameter tuning for all
274 bias correction and predictions to ease comparability between the outcomes.

275 Once the hyperparameter tuning is done and prior to performing the final bias-correction, we
276 test if the bias-correction is beneficial for palliating to the models' bias and if it also benefits from
277 training the regressors at the daily time-step or if a training using the time-mean bias is sufficient.
278 To perform this evaluation using the same metrics as in the model evaluation, we bootstrap each
279 regressors 25 times per day, randomly sampling 80 % of the PWS locations that had data available
280 on that day as training and keeping the remaining 20 % as testing – for both the daily-minimum,
281 -maximum and -average, and their respective summer time-mean average. We then first average all
282 bootstrapped T2_BC at the testing PWS sites before performing a subsequent averaging to obtain
283 an average T2_BC at the daily time step representative of all randomly selected testing PWS sites.
284 These are evaluated against the daily average of all observed temperature at the PWS sites – for

285 daily minimum, maximum and average. In short, we are measuring how well do the two different
286 types of bias correction perform under all regressors for capturing the daily variation (n=92 days)
287 of temperature on average.

288 After this final step, we bias-correct both the BouLac and the YSU runs using 100 % of the
289 measured biases and related covariates at PWS locations to compare the spatial outcomes. We
290 also predict T2 out of PWS' observed T2 with the same set of covariates used to predict the model
291 bias to illustrate how divergent each bias-corrected model outputs are to a simplified predicted T2
292 that is not a derivative of any model constraint. Because more refined and complex techniques
293 exist to predict air temperature from PWS and very high-resolution earth observations (e.g., Venter
294 et al. (2020), Venter et al. (2021)), we do not evaluate these predicted temperatures which should
295 simply be considered as an illustration of how bias-corrected products are similar or divergent to
296 observational data.

297 Lastly, to illustrate the potential benefit of modelled air temperature bias-correction prior to
298 urban heat impact studies, we calculate the average population weighted temperatures – based on
299 the United Kingdom census data from 2011 – in Greater London before and after the bias-correction.

300 **3. Results**

301 *a. WRF simulation evaluation*

302 When we evaluate the two model simulations against MIDAS official weather stations only, they
303 perform similarly, demonstrating a systematic negative bias of ~ 0.55 °C on average (Table 3). The
304 average correlation with the automatic weather stations following the squared Pearson's r^2 is of
305 0.77 for BouLac and 0.79 for YSU, while using Spearman's r it is of 0.86 and 0.88, respectively. A
306 slight decreased performance is found in urban pixels for YSU, with an average MAE of 1.83 °C
307 and a negative MB of 0.79 °C compared to BouLac's 1.82 °C for MAR and -0.56 °C for MB.
308 In general, the bias is more important at night, and, in non-urban stations, performances are
309 similar. Hence, looking only at the models' performances using standard in-situ observations
310 doesn't provide information on which model represents the urban climate more accurately.

315 On the other hand, comparison with PWS observations identifies differences in performance in
316 urban areas between the models, as shown by the performance metrics plotted in Figure 3 and C1.
317 The BouLac simulation has a stronger cool bias of -1.46 °C \pm 0.6 °C on average in the urban area,

311 TABLE 3. Average of all performance metrics calculated at each MIDAS official weather stations for hourly air
 312 temperature at 2 m for the summer period (1st June 2018 to the 31st of August 2018). Urban stations are stations
 313 located in a pixel classified as an urban LCZ in WRF and rural stations are located in other natural land-use
 314 land-cover.

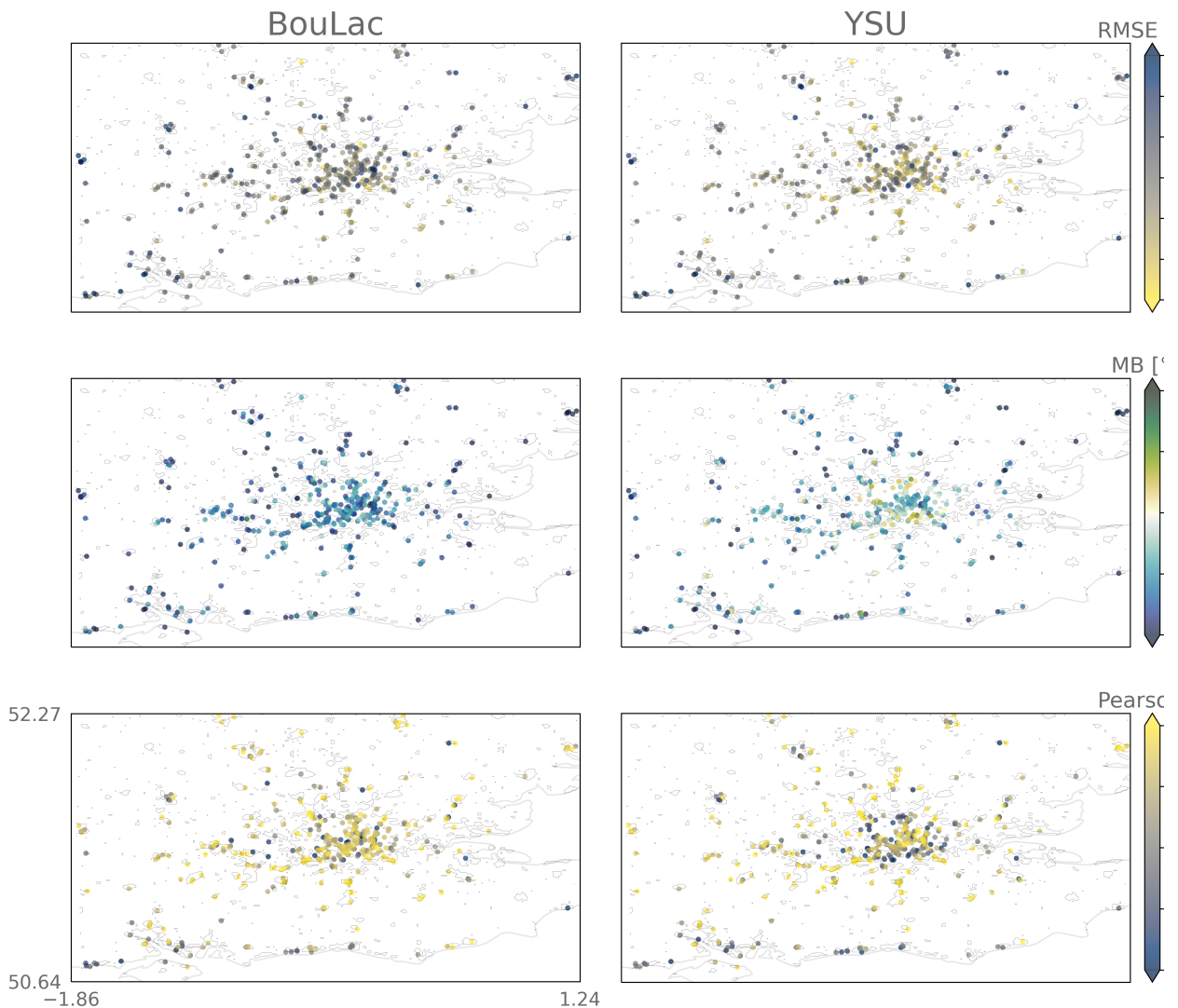
	BouLac					YSU				
	RMSE	MAE	MB	r ²	r	RMSE	MAE	MB	r ²	r
All	2.33	1.82	-0.56	0.77	0.86	2.31	1.83	-0.57	0.79	0.88
Urban	2.42	1.88	-0.73	0.76	0.86	2.42	1.92	-0.93	0.77	0.87
Rural	2.32	1.81	-0.53	0.78	0.86	2.28	1.81	-0.50	0.80	0.88

318 compared to YSU’s MB of $-0.97\text{ °C} \pm 0.81\text{ °C}$. RMSE and MAE are similar, with values of 2.79 °C
 319 $\pm 0.36\text{ °C}$ and $2.19\text{ °C} \pm 0.31\text{ °C}$ for BouLac and $2.65\text{ °C} \pm 0.40\text{ °C}$ and $2.14\text{ °C} \pm 0.34\text{ °C}$ for
 320 YSU. These metrics are consistent with the MIDAS observations, highlighting a systematic cool
 321 bias of the model and a coefficient of determination (r²) of 80 %. Importantly, the variability in
 322 the model’s performance is more greater in the YSU run – reflected by greater standard deviations
 323 of performance metrics – and, in the BouLac simulation, the metrics are more heterogeneously
 324 distributed amongst the urban area. Indeed, when we look at the YSU simulation, we can see
 325 that the model has a smaller MB in suburban areas and a greater MB in the city centre. Yet, in
 326 parallel, the correlation with the PWS is lower in the suburban areas and higher in the centre of the
 327 city. This could mean that YSU accurately represents the urban temperatures on average due to
 328 compensating effects, which we do not intend to evaluate in this study. Nevertheless, this shows
 329 how PWS are beneficial for capturing the spatial heterogeneity of each model’s performance and
 330 therefore supports the use of spatially-varying bias-correction.

337 *b. Bias correction of urban climate simulations*

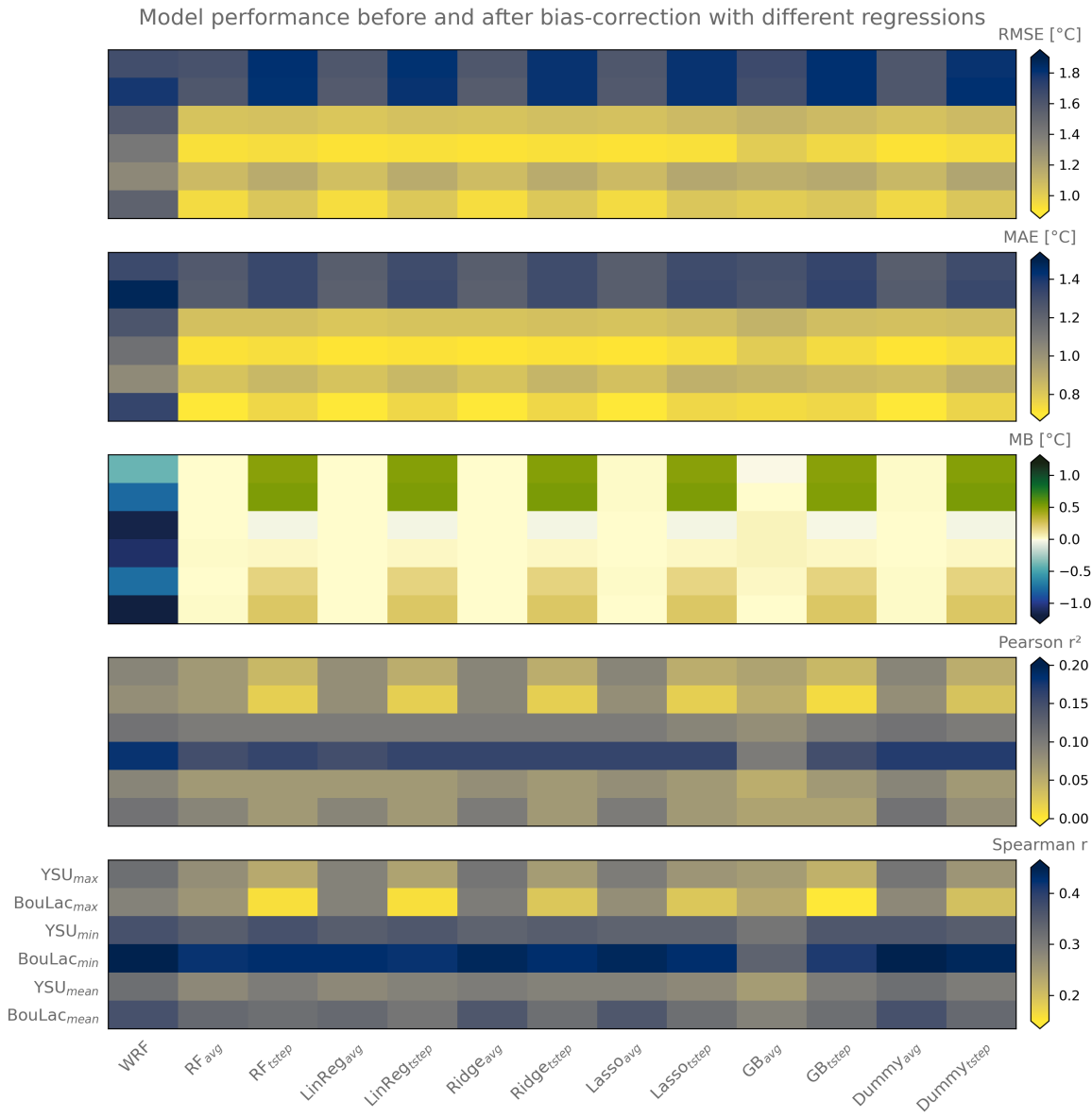
338 Over our domain of study covering south-east England during the Summer 2018, both models
 339 are subject to a cold negative bias of $\sim -0.5\text{ °C}$ on average according to official stations and of
 340 $\sim -1.0\text{ °C}$ to $\sim -1.5\text{ °C}$ according to PWS. But as demonstrated above, the bias of the models against
 341 PWS observations has substantial spatial variation and so the bias correction for urban heat impact
 342 studies should be spatially explicit.

348 We find that each machine learning regressors give similar performance (Figure 4; values numer-
 349 ically given in Tables C1 and C2). All bias-corrections were however beneficial compared to the



331 FIG. 3. Performance metrics calculated at location of each citizen personal weather station (PWS) for the
 332 two model simulations using different planetary boundary layer schemes (YSU and BouLac). The metrics are
 333 calculated over the whole summer 2018 with hourly outputs of near surface air temperature at 2 m. Root
 334 mean square error (RMSE) and mean bias (MB) are given in degrees Celsius ($^{\circ}\text{C}$). Coeffecients of correlation
 335 measured with the squared Pearson's r are also provided. Mean absolute error (MAE) and Spearman's r are given
 336 in Figure C1 to increase clarity.

350 original outputs from the WRF model, reducing RMSE, MAE and MB by 0.29°C , 0.32°C and
 351 1.02°C on average. The bias-correction was most efficient for daily-minimum temperatures and
 352 less for daily-maximum temperatures, where RMSE was not diminished – if not slightly increased

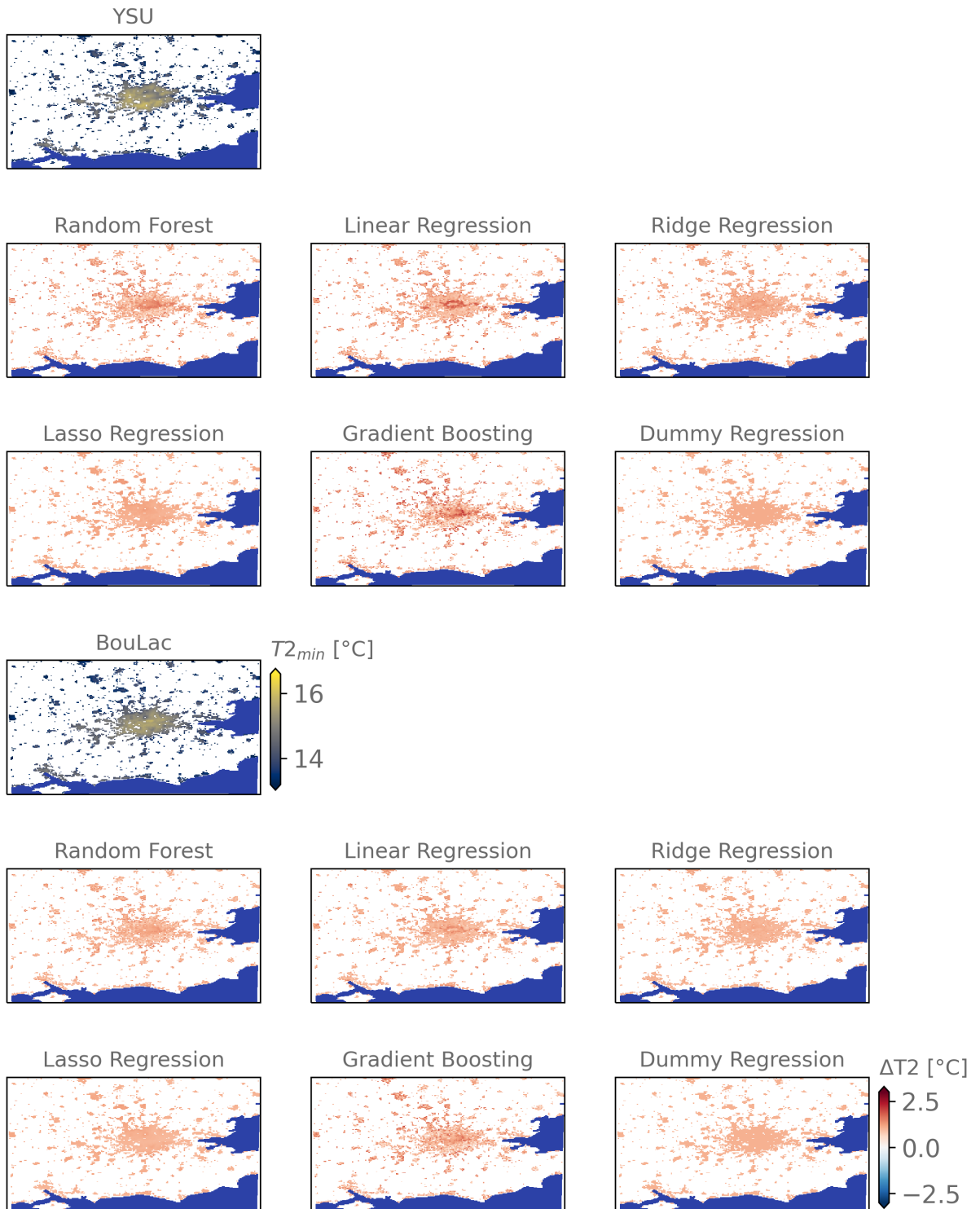


343 FIG. 4. Performance metrics for the model prior to the bias-correction (WRF) and all the different regressions
 344 (random forest: RF; linear regression: LinReg; Ridge regression: Ridge; Lasso regression: Lasso; gradient
 345 boosting: GB; and dummy regression: Dummy). The different regressions are assigned a suffix: “avg”
 346 for regressions that were trained on the summer time-mean average of daily-minimum, -mean or -maximum
 347 temperatures, and “tstep” for those that were trained with the temperatures at each daily time-step.

353 (by 0.05 °C for YSU daily-maximum temperatures for example) – by the time-step bias-correction.
354 Interestingly, the spatial correlation between the bias-corrected and the observed temperatures are
355 low, with values ranging from around 0.02 to 0.2 for the squared Pearson’s r and from around 0.15
356 to 0.45 for Spearman’s r. This can be expected as machine learning algorithms have difficulties rep-
357 resenting a time-varying variable with static spatial elements only (Georganos et al. 2021; Venter
358 et al. 2021). Unexpectedly, we find that the training at the daily time-step does not outperform the
359 training at the summer time-mean in terms of spatial correlation with the heat distribution across
360 London. Nonetheless, if we take the average daily-minimum, -mean and -maximum temperatures
361 of all PWS and compare it to the modelled temperatures, we find that the time-step bias-correction
362 is closer to the observations (Figures C2 to C4). Lastly, we find that greater model performance
363 is achieved with a minimum of ~24 % (96 PWS) of the whole sample of PWS and that official
364 weather stations are detrimental to the regressors performance (see Appendix B).

365 Comparing the spatial differences of the bias-corrected products related to the complexities of
366 each regressors, we find that although each regressor is performing similarly on average, important
367 disparities are found between the outputs. For example, when looking at the average bias-correction
368 imposed to daily-minimum temperatures after training the regressors at each time-step, the Lasso
369 and the Ridge regressors impose a flat bias-correction, similar to the dummy regression, while the
370 random forest and gradient boosting regressors’ degrees of freedom result in a spatially diverse
371 bias-correction (Figure 5 and Figures C5 and C6). Besides, the linear regression imposes an average
372 bias-correction spatially-correlated to the modal LCZ. In general, the signal is consistent across
373 each regressors, apart from the Lasso and the dummy regression, where, for YSU, central London
374 requires a stronger bias-correction by 1 °C to 2 °C compared to the suburban areas where the
375 bias-correction is around 0.5 °C ; for BouLac, the central bias-correction is lower than YSU. We
376 find that these spatial tendencies are also found for daily-maximum and daily-average temperatures,
377 defending our hypothesis of a systematic bias correlated to spatially explicit input parameters. The
378 spatial differences in bias-correction are however less important for daily-maximum temperatures,
379 which is the time at which the urban heat island is also expected to be the lowest.

Modelled temperatures and respective bias-corrections with multiple regressors



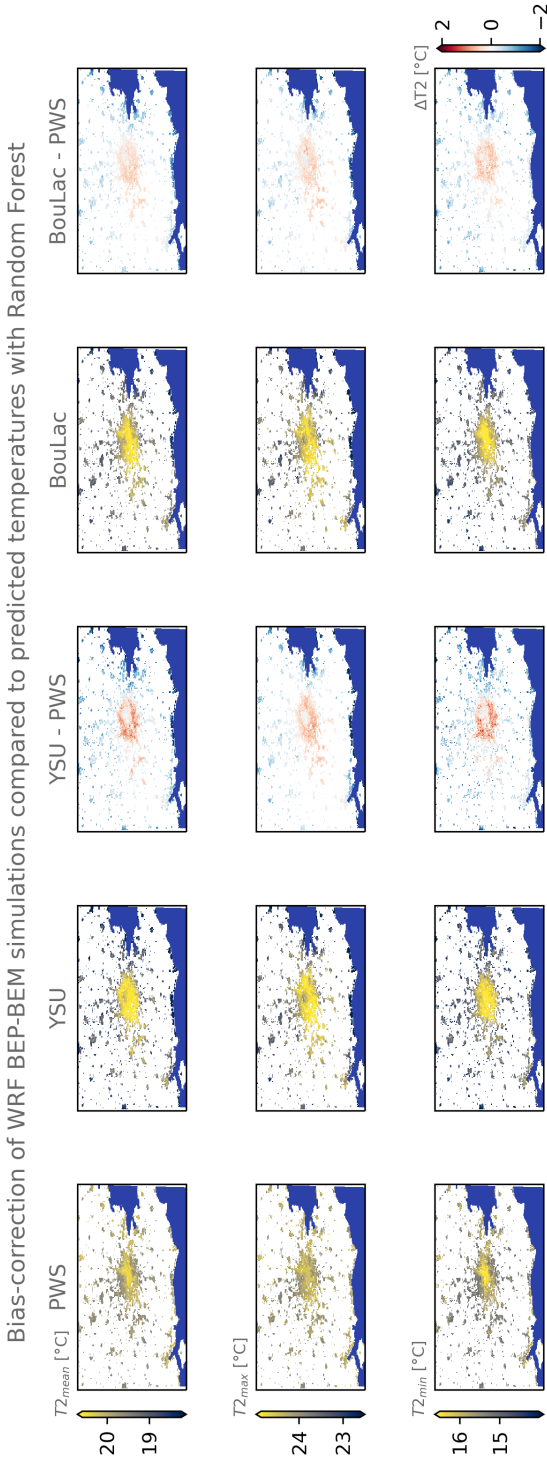
380 FIG. 5. All regressions propose different bias-corrections (ΔT_2) of the average modelled absolute daily
381 minimum urban temperature ($T_{2_{min}}$). Differences of bias-correction are observed between the runs with different
382 planetary boundary layer schemes (Bougeault-Lacarrère – BouLac, and Yonsei University – YSU). The centre
383 of London is subject to a stronger bias-correction. Rural lands are masked in grey and the seas in blue. Bias
384 corrections of daily mean and maximum temperatures are given in Figures C5 and C6

385 Finally, we find that the bias-corrected BouLac simulation corresponds spatially to predicted
386 temperatures using PWS more than YSU – something we find equally across all regressors (Figure 6
387 and Figures C7 to C11). As an example, when comparing the average bias-corrected products
388 using the time-step trained random forest regressor we can see that YSU urban heat is more
389 homogeneously distributed than BouLac’s or the predicted temperatures from PWS only. BouLac’s
390 bias-corrected product shows stronger urban heat in central London compared to suburban areas,
391 coherent with the predicted temperatures. Nonetheless, BouLac’s suburban areas are hotter by
392 0.5 °C to 1.0 °C than the predicted ones with PWS only. This remains less pronounced than in
393 YSU. Lastly, we can see that both bias-corrected products show similar trends when compared
394 to the PWS-only predicted temperatures with hotter suburban areas and cooler secondary cities
395 as well as coastlines. Again, this does not show which product between the PWS-only predicted
396 temperatures and the bias-corrected products is better since we do not evaluate this here.

403 These results show that bias-correction of modelled air temperature change their spatio-temporal
404 distributions. When focusing on the potential impact bias-correction may have in estimated urban
405 heat impact on urban health, we find that using the random forest regression trained at each daily
406 time-step leads to an increased average population weighted temperature by 0.77 °C in the YSU
407 case, and of 1.24 °C in the BouLac case. Raw model outputs are thereby lowering the impact of
408 heat on the urban population.

409 4. Discussion

410 In this study, we argue that the joint use of crowd-sourced personal weather stations (PWS) and
411 urban climate models (UCMs) can add value to urban climate research and in particular to urban
412 climate impact research. This is supported by two major outcomes of our case-study focused over
413 London during the summer 2018. First, we showed that evaluation of urban climate simulations
414 using PWS enables the detection of spatially-varying systematic biases in urban areas related to the



397 Fig. 6. The random forest regressor leads to different bias-corrections of the two WRF simulations parameterized with different turbulence schemes
 398 – the Yonsei University (YSU) and the Bougeault-Lacarrère (BouLac) – and with the BEP-BEM urban canopy model activated. This holds for average
 399 daily mean, minimum and maximum temperatures (T_{2_mean} , T_{2_min} and T_{2_max}) after the daily time-step bias-correction. Compared to the predicted
 400 temperatures using the personal weather stations data only (PWS), the bias-corrected products are hotter in the suburban areas of the Greater London and
 401 cooler in the rural areas. The difference is more pronounced in YSU (see YSU – PWS). Greyed areas represent natural areas where the bias-correction
 402 is not performed and the sea is shown in dark blue. The same figures for the other regressors are given in Figures C7 to C11

415 UCMs’ parameterization, which are not detectable using only official weather stations. Second,
416 we demonstrated that PWS, combined with detailed morphological data derived from LCZ maps,
417 can be used to derive a spatially varying bias-correction via commonly used machine-learning
418 regressors. This latter point has major implications for urban climate impact research – and
419 especially future urban climate impact studies – as we hereby propose the first bias-correction
420 technique that considers the existence of a non-linear spatially heterogeneous bias in modelled
421 urban climates.

422 Of course, using PWS for evaluating UCM simulations should always cautiously be considered
423 because of the lower accuracy of PWS and the potential uncertainties related to user-driven mistakes
424 in the set-up of their PWS (e.g., indoor sensors instead of outdoor, poor shading conditions, height
425 of the sensor, etc.). However, reliable tools have now been developed since the first use of PWS for
426 model evaluation by Hammerberg et al. (2018) to filter dubious measurements out (e.g., *CrowdQC*
427 from Napoly et al. (2018) or *CrowdQC+* by Fenner et al. (2021)), thus making PWS observations
428 increasingly reliable. This does not resolve the question of the representativity of measurements,
429 i.e., “how is one PWS measurement representative of the simulated urban pixel?” Yet, the increasing
430 density of PWS in the urban environments begins to alleviate this uncertainty – despite a recognised
431 unequal distribution of PWS amongst a variety of environmental, socio-economic and demographic
432 indicators (Brousse et al. 2023). For example, Venter et al. (2020) found that a density of one
433 PWS per square kilometre is optimal for predicting seasonal air temperature in Oslo. Dense PWS
434 networks hence permit the detection of systematic biases that would otherwise pass undetected.
435 Therefore, to support the development of PWS as a source of urban weather observations for model
436 evaluation, urban climate scientists should identify an optimal density of PWS for UCM evaluation,
437 to define which cities are in need of urban weather observations, and to start instigating common
438 frameworks and standards.

439 We consider our study innovative and supportive of future advances in the field because it is the
440 first bias-correction technique in urban environments which considers that UCMs’ simulated UHI is
441 spatially heterogeneous in its accuracy and that the UHI is not solely linearly correlated to the urban
442 fraction. Aided by the expanding fields of crowd-sourcing weather observations through PWS,
443 machine learning, and potentially deep learning, we infer that our work should serve as the basis of
444 future research that would try, but not restricted to, improving the bias-correction of urban climate

445 models using PWS. For instance, we did not find any machine learning regressor to be more efficient
446 at predicting the model bias. This could be explained by the rather restricted set of covariates we
447 used for training the regressors as well as the coarse horizontal resolution of 1 km at which the
448 covariates were aggregated to be consistent with the model's spatial resolution. Higher spatial
449 resolutions and more specific satellite earth observations could be used to improve regressors'
450 performance, following up on the work by Venter et al. (2021), for example. When modelling the
451 near-surface UHI, which is not a model bias, their regressor achieved similar performances as ours,
452 with an RMSE of 1.05 °C and a Pearson's r^2 of 0.23. Although the common use of model's input
453 parameters and earth observations as covariates could be beneficial, a particular attention should
454 be given to the choice of earth observations since these should not be decorrelated to the model's
455 physics and dynamics as the purpose would remain the bias-correction.

456 Independent of the set of covariates used in this study we found that the regressors performances
457 greatly improved when trained over a certain number of PWS (more than ~90) before plateauing.
458 Because of this, future research should try to investigate how machine learning regressors could
459 benefit from unfiltered PWS data and other PWS data sources. Interestingly, we found that official
460 sources of data like MIDAS were detrimental to the regressors, potentially because official weather
461 stations tend to be placed in open fields or parks without surrounding built-up areas to increase
462 measurement accuracies. This would explain why our regressors tended to further increase the
463 systematic cool bias when using only MIDAS stations for training as parks are typically cooler at
464 night and on average than more urbanised areas where PWS are located. In addition, we found
465 that training regressors at the daily time-step did not outperform a training with the summer time-
466 mean average. Regressors could therefore gain in performance by adding a temporal component
467 to the covariates. Following up on this idea, the recent work by (Zumwald et al. 2021) tried
468 predicting the near-surface air temperature in Zurich for the 30th of June 2019 out of ~650
469 Netatmo PWS' measurements during the preceding week. Their set of covariates consisted of
470 spatial earth observations as well as 35 meteorological predictors that were all derived from one
471 official automatic weather stations. The latter predictors helped training the model to recognise
472 how the temperature measured at each PWS location was related to the meteorological variables
473 measured at the automatic weather stations. Their predictions at hourly time-steps achieved
474 reasonable performances with RMSEs around 1.70 °C. Bias-correction of UCM simulations could

475 hence be improved by incorporating temporally explicit meteorological observations from official
476 weather stations. Notwithstanding, this would require extensive investigation on the area down
477 to which each official station is representative for training the regressors. More geographically
478 oriented machine learning regressors, like the geographical random forests (Georganos et al. 2021),
479 could also help integrate these spatial heterogeneities for an improved bias-correction.

480 In general, we support the use of PWS observations for bias-correction of urban climate simula-
481 tions. As shown in this case study, model outputs prior to any bias-correction could lead to under-
482 or over-estimation of urban heat impact on public health. We indeed find that for the summer 2018
483 in London, average population weighted temperatures were higher after bias-correcting the model
484 outputs, suggesting higher urban heat related mortality during this period. This simple example
485 shows that bias-correction of urban climate simulations could have important implications for
486 calculating the exposure of urban citizen to heat or estimating the urban heat-related mortality.
487 Although preferring bias-corrected model outputs to predicted urban air temperatures from earth
488 observations for present-day urban heat impact studies is not covered in this study – and must be
489 further explored – we still argue that bias-correction should be done prior to any urban heat impact
490 studies that imply using climate model outputs. This argument is especially valid for future climate
491 projections at urban scale and we encourage future research to investigate how to transfer present
492 urban bias-correction coefficients to simulated future urban climates. Doing so, bias-corrected
493 simulations could help targeting areas where heat mitigation or adaptation strategies could be more
494 beneficial as their efficiency is dependent on their location and scales of implementation (Yang and
495 Bou-Zeid 2019; Broadbent et al. 2022). We also suggest that our methods could be extended to
496 other fields of urban climatology and urban air quality. Several devices already offer the possibility
497 to obtain information on air quality, precipitation or wind speed, to name a few (De Vos et al. 2020).
498 Hence bias-correction of regional climate models’ outputs using crowd-sourced data should not be
499 restricted only to air temperatures.

500 **5. Conclusions**

501 We demonstrate that the higher density of personal weather stations (PWS) measurements of
502 temperatures in cities like London is beneficial for urban climate model evaluation. We then show
503 that PWS could be helpful for bias-correcting modelled temperatures using a set of machine learning

504 statistical regressors. We did not observe tangible differences in performance of the regressors
505 to predict the bias at various locations. A minimum of ~24 % of the total sample size of PWS
506 (96 stations of the 402 used in this study) was required to efficiently train our regressors; official
507 weather sources like MIDAS were detrimental to the urban bias-correction, probably because of
508 site specificities. Our work has important implications for urban climate impact studies that would
509 make use of urban climate model outputs.

510 *Acknowledgments.* We personally thank Stefanos Georganos for his help and his comments on
511 machine learning classifiers and regressors. We also thank Daniel Fenner and Fred Meier for their
512 valuable insights concerning data acquisition, filtering and treatment of crowd-sourced citizen
513 weather stations. Lastly, we are grateful to Matthias Demuzere and other committed members of
514 the WUDAPT project for providing the European LCZ map and the python W2W tools. CH is
515 supported by a NERC fellowship (NE/R01440X/1) and acknowledges funding for the HEROIC
516 project (216035/Z/19/Z) from the Wellcome Trust, which funds OB and CS.

517 OB designed the study and led the conception of the manuscript with the support of CH and
518 CS. OB was responsible for the WRF modelling, the model evaluation and the bias-correction.
519 CS provided support in the python coding and in the statistical analysis for the bias-correction.
520 OK was responsible for technical support of the installation of WRF on the University College
521 London's "Kathleen" and "Myriad" super-computers. AZ and AM offered guidance in the set-up
522 of the WRF model v4.3 and urban heat modelling expertise with SK. All authors contributed to
523 the writing of the manuscript.

524 The authors declare no conflicts of interest.

525 *Data availability statement.* The simulations done in this research were performed using the WRF
526 model v4.3 (<https://github.com/wrf-model/WRF.git>). The scripts and WRF namelists used
527 in this study are accessible at [https://github.com/oscarbrousse/JAMC_BiasCorrection_](https://github.com/oscarbrousse/JAMC_BiasCorrection_PWS/)
528 [PWS/](https://github.com/oscarbrousse/JAMC_BiasCorrection_PWS/). The related outputs presented in this research available upon reasonable request addressed
529 to the corresponding author.

APPENDIX A

Model sensitivity testing over the two hottest days of Summer 2018

Prior to running the 3-months simulation, we tested the model's sensitivity to a set of parameterization to assess which model is the best performing model for the 3-months simulation. We perform the sensitivity in a progressive way; parameters are kept if beneficial, removed if detrimental. We chose to run the simulations over the two hottest days of the summer 2018 with one additional day as spin-up time – from the 25th to the 27th of July 2018 – to see how the model is capable of accurately representing an extreme condition in terms of air temperature at 2 m – tested against official MIDAS automatic weather stations and personal Netatmo PWS. The model was also tested for relative humidity and wind speed at 10 m at MIDAS locations where records were available. All wind-speed measurements are converted from knots to $\text{m}\cdot\text{s}^{-1}$.

We start from Heaviside et al. (2015) model's parameterization, who simulated the impact of urbanization on the local climate in the West Midlands in England, but supplement the CORINE land-use land-cover by the Local Climate Zones classification instead since Brousse et al. (2016) compared both products and proved the added value of LCZ over Madrid. We chose the work by Heaviside et al. (2015) as a starting point since it also uses the BEP urban climate model, coupled to the WRF model and is one of the only WRF simulations done over England.

From there, our simulations tested: i) the use of YSU, recently coupled to the BEP-BEM model (Hendricks et al. 2020), instead of Bougeault-Lacarrere; ii) the use of the more complex land surface scheme Noah-MP in its default parameterization instead of the default Noah land surface model; iii) the forcing by ERA5 reanalysis data at 25 km horizontal resolution instead of ERA-Interim; iv) the reduction of soil moisture by 50 % and its increase by 200 %, following suggestions provided by Martilli et al. (2021). We chose not to test the impact of urban canopy parameters in this case to keep our simulations standardized and universally coherent through the LCZ scheme. Their simulation used the same micro-, clouds, convection and radiation physics than ours.

We found that all steps taken from the original parameterization by Heaviside et al. (2015) were beneficial to the model's performance. Through an intermediate simulation where we tested again the BouLac turbulence scheme after step iii, we found that YSU was still performing better.

APPENDIX B

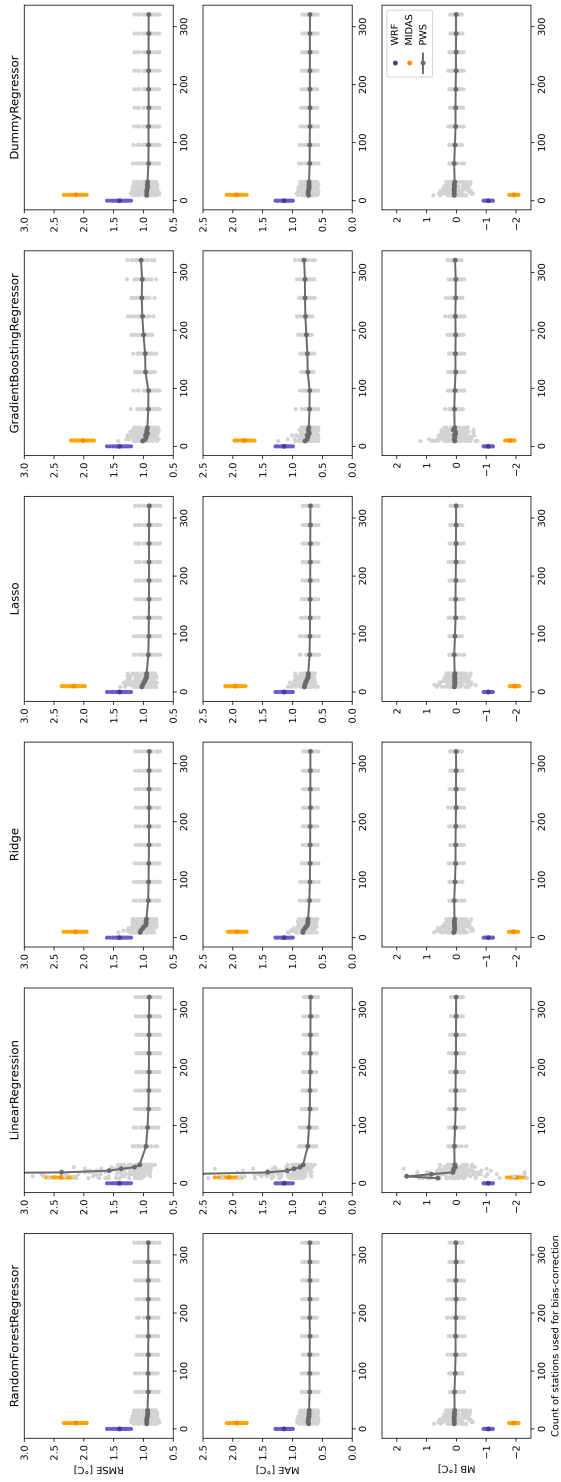
Sensitivity of machine learning regressors to data quality and quantity

Before running our bias-correction and our bootstrapping we needed to evaluate the degradation in performance of all the regressors in relation to the quantity of data available for training. This way, we could ascertain that the chosen amount of 80 % for running the bootstrapping procedure was not detrimental to the regressors' performances. Additionally, despite the fact that official weather data coming from MIDAS is usually coming from open fields like airports or parks, we still chose to test how our model performs if only this data was available for bias-correction; thereby ensuring that the use of the dense network of PWS is useful for bias-correction. To test this we trained all the regressors over both WRF boundary layer conditions to bias-correct the summertime average daily mean, minimum and maximum temperatures. This means that we are testing the ability of the regressors to predict the bias at certain PWS locations to correct the modelled temperature. In this case, we evaluate the bias-corrected temperatures against the observed temperatures. We chose not to run over daily time steps as this would be too computationally expensive.

We followed a bootstrapping procedure, where 20 % of the PWS temperature data were randomly selected and kept for testing the regressors performance. Random samples with increasing ratios of the remaining 80 % of PWS temperature data and covariates were used to train the regressors 25 times. We ensured that the randomly sampled 20 % and ratios are kept constant between regressors. We first started with 1 % of the remaining 80 % and increased the ratio by steps of 1 % until 10 % of the remaining 80 %. Steps of 10 % were then used until reaching 90 % of the remaining 80 %. We chose to use these steps as we expect our regressors performance to rapidly increase with a low amount of data before plateauing with a greater amount of data. Then, to test the added value of urban PWS density and data we trained the same regressors over the modelled bias at the 10 urban MIDAS stations locations and evaluated the bias correction against the 20 % of the PWS data kept for evaluation at each bootstrapping step. As a comparison, we also evaluated the WRF output prior to bias correction against the same 20 % of PWS temperature data at each bootstrapping step to demonstrate the added value of bias correction using a certain amount of PWS.

We found that all regressors benefited from a greater amount of PWS data which reduced the root mean squared error (RMSE), the mean absolute error (MAE) and the mean bias (MB) on average and also reduced the variability of performances between each bootstrap sample. Only

588 gradient boosting showed a slightly deteriorated performance by having more than 30 % of the 80 %
589 PWS data used for training (96 PWS) – probably due to overfitting. Below 40 PWS, all models
590 performed poorly. We also showed that training the regressors over official MIDAS data only led
591 to a poor bias correction for both summertime average daily minimum and mean temperatures.
592 For the maximum, no clear benefit was demonstrable, which was also the case with PWS and
593 which could be explained by the lower UHII during hot hours of the day, as discussed in the
594 manuscript. We argue that this general outcome is explicable by the standard location of MIDAS
595 weather stations – typically located in open parks or fields – which would explain why the bias
596 correction for minimum temperatures further increases the cool bias already existing in WRF. This
597 supports the use of PWS for bias correction of urban temperatures for two reasons: first, the need
598 for a sufficiently dense network of weather stations in urban environments; second, the necessity
599 of weather stations located in typical built-up environments to accurately represent the effect of
600 built-up surfaces on the local climate.



601 **Fig. B1.** Regressors performance for bias correction of the summer average daily-minimum air temperature depending on the amount of weather
 602 stations' used for training. The performance is evaluated with the mean absolute error (MAE; in °C), root mean squared error (RMSE; °C) and mean
 603 bias (MB; °C). Blue dots represent the WRF model performance prior to bias-correction, in orange are the performance of the WRF model after
 604 bias-correction using MIDAS official weather stations, and in grey are the performance of the WRF model after bias-correction using subsets of the
 605 available Netatmo personal weather stations. Small lighter dots are representative of performances measured at each bootstrapping steps (n=25) and
 606 large darker dots are the average of all bootstraps. Here the WRF model was run with the Bougeault-Lacarrère boundary layer scheme (BouLac).

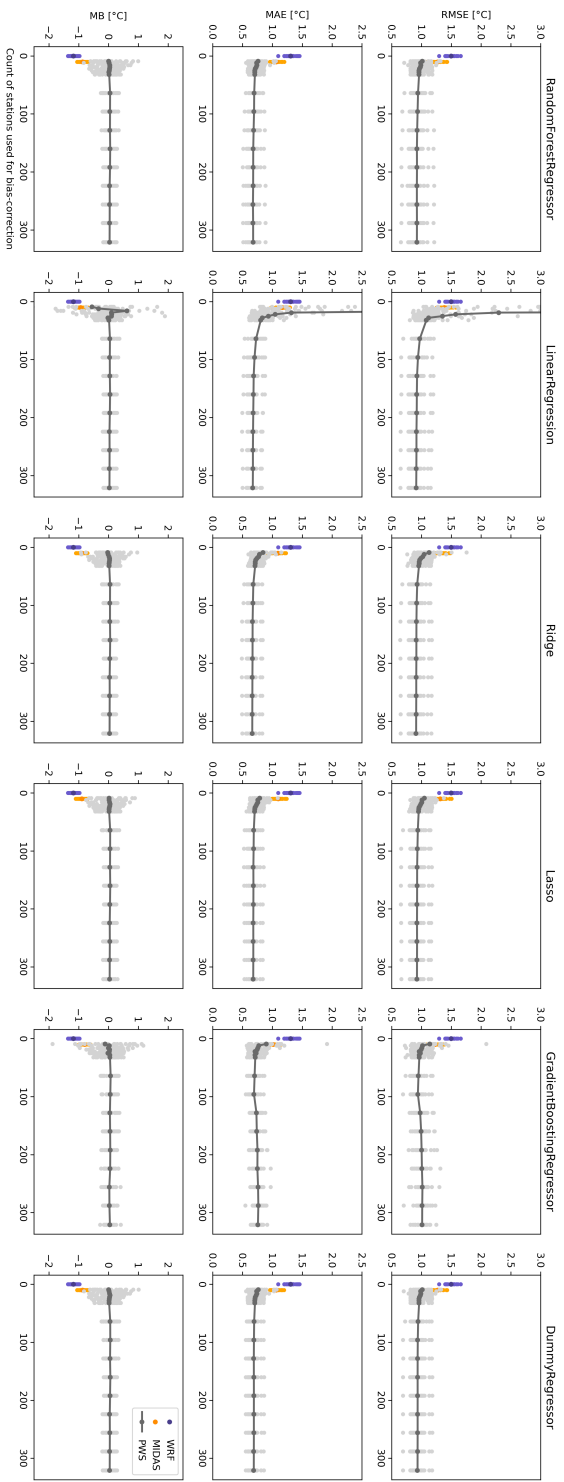


FIG. B2. Same as Fig. B1 but for summer average daily-mean temperatures.

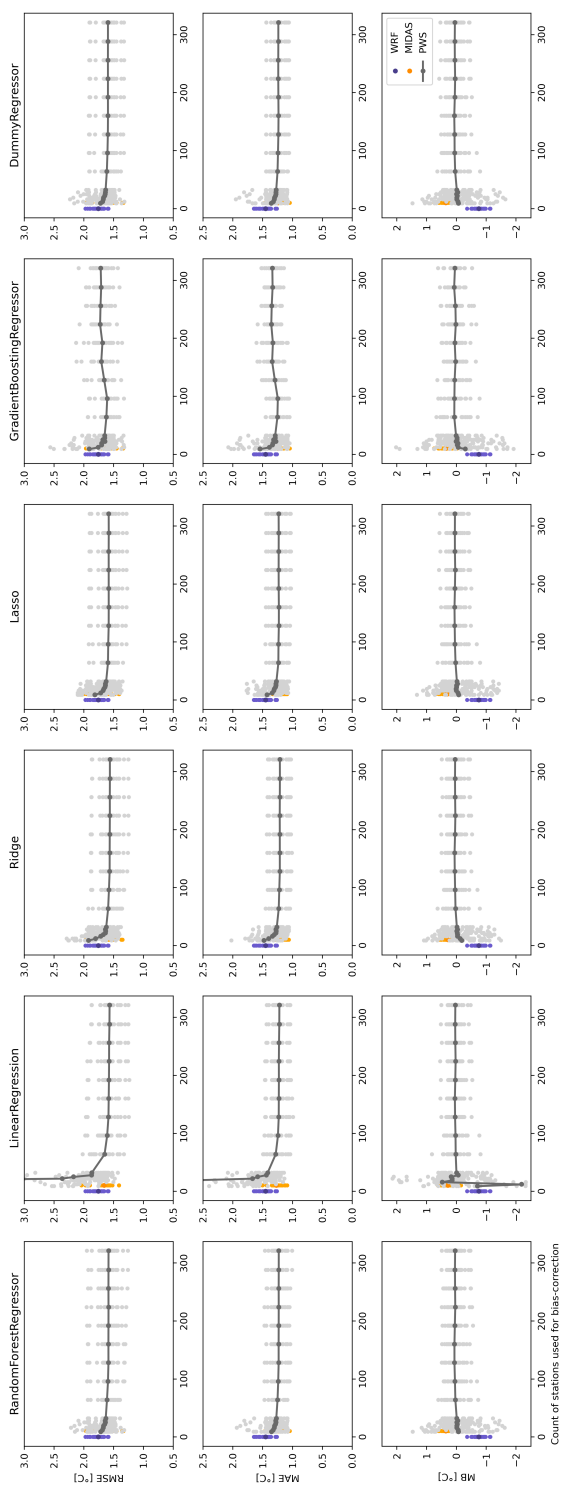


FIG. B3. Same as Fig. B1 but for summer average daily-maximum temperatures.

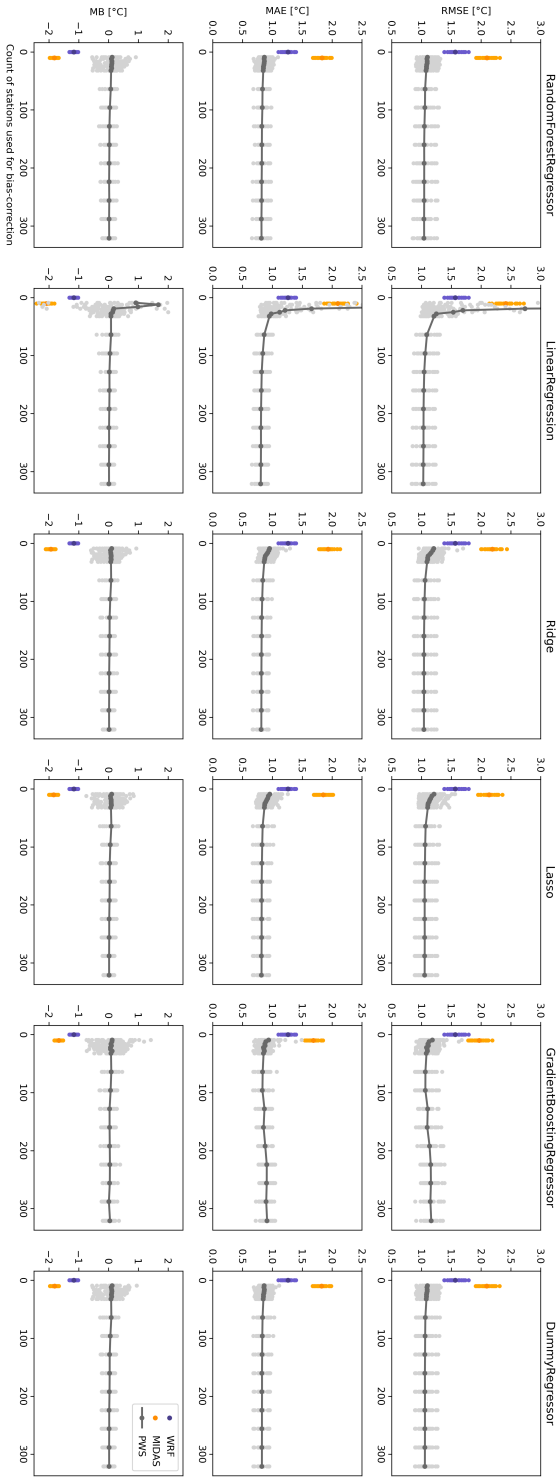


FIG. B4. Same as Fig. B1 but WRF model used the YSU planetary boundary layer scheme.

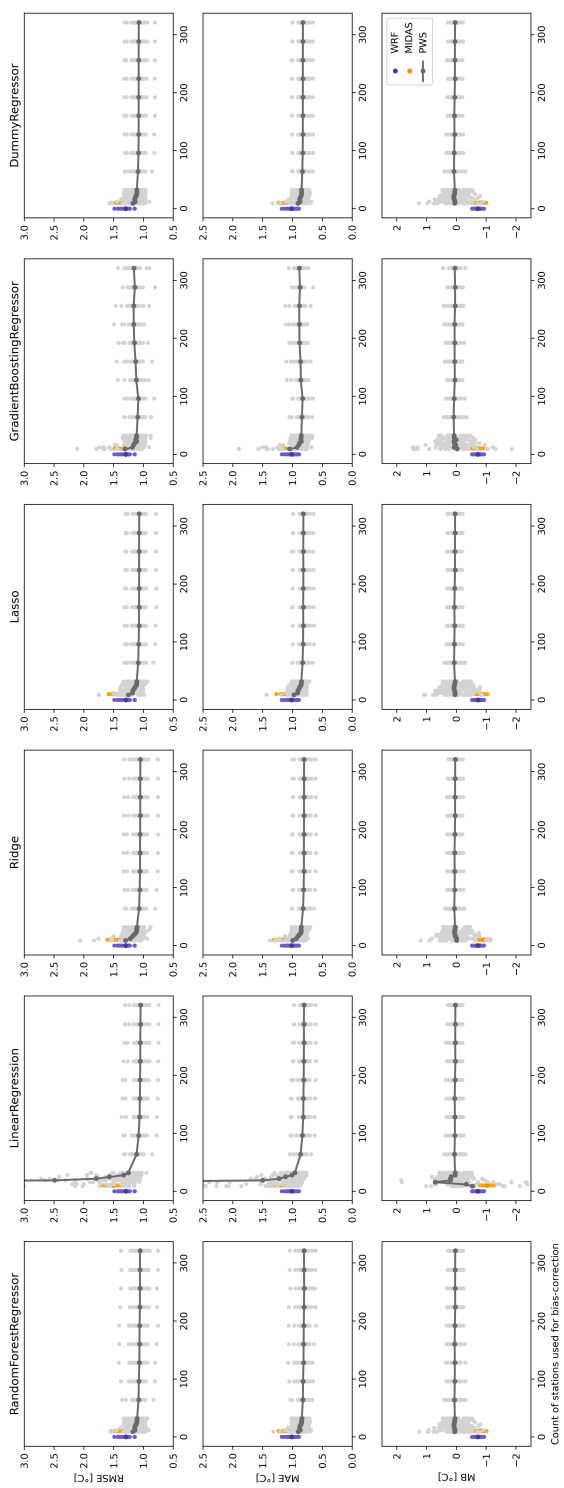


FIG. B5. Same as Fig. B4 but for summer average daily-mean temperatures.

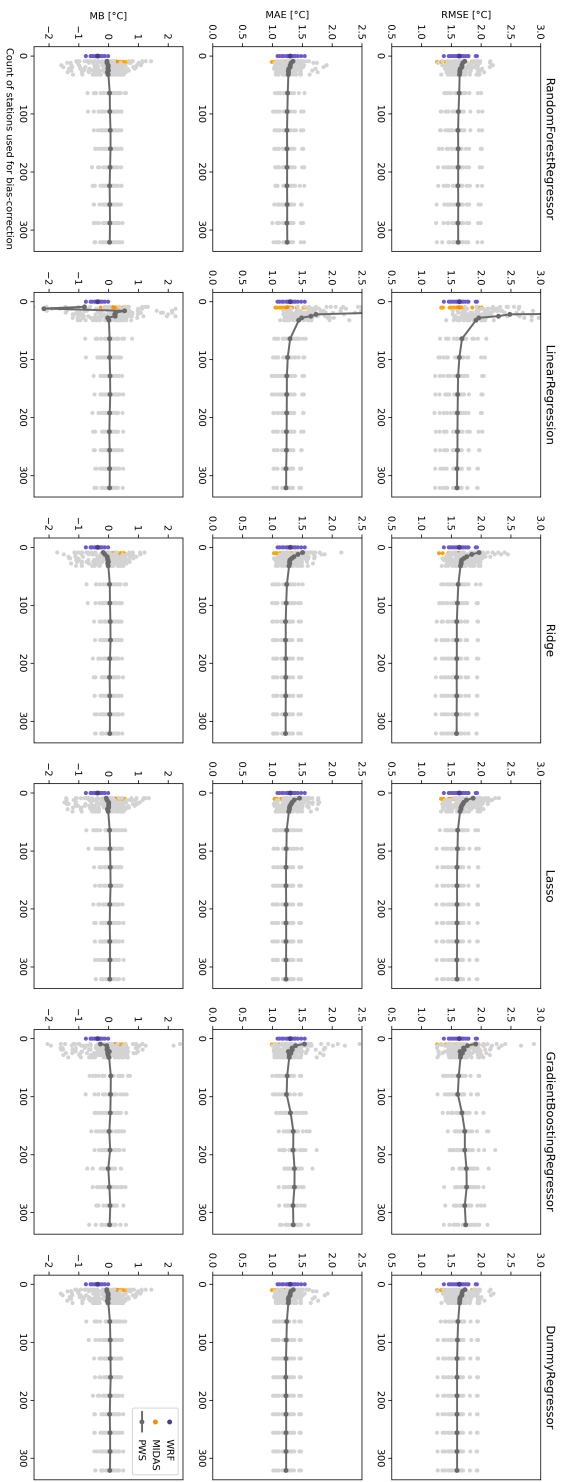


FIG. B6. Same as Fig. B4 but for summer average daily-mean temperatures.

607

APPENDIX C

608

Additional Figures and Tables

609

This section presents all the figures that are not given in the main text.

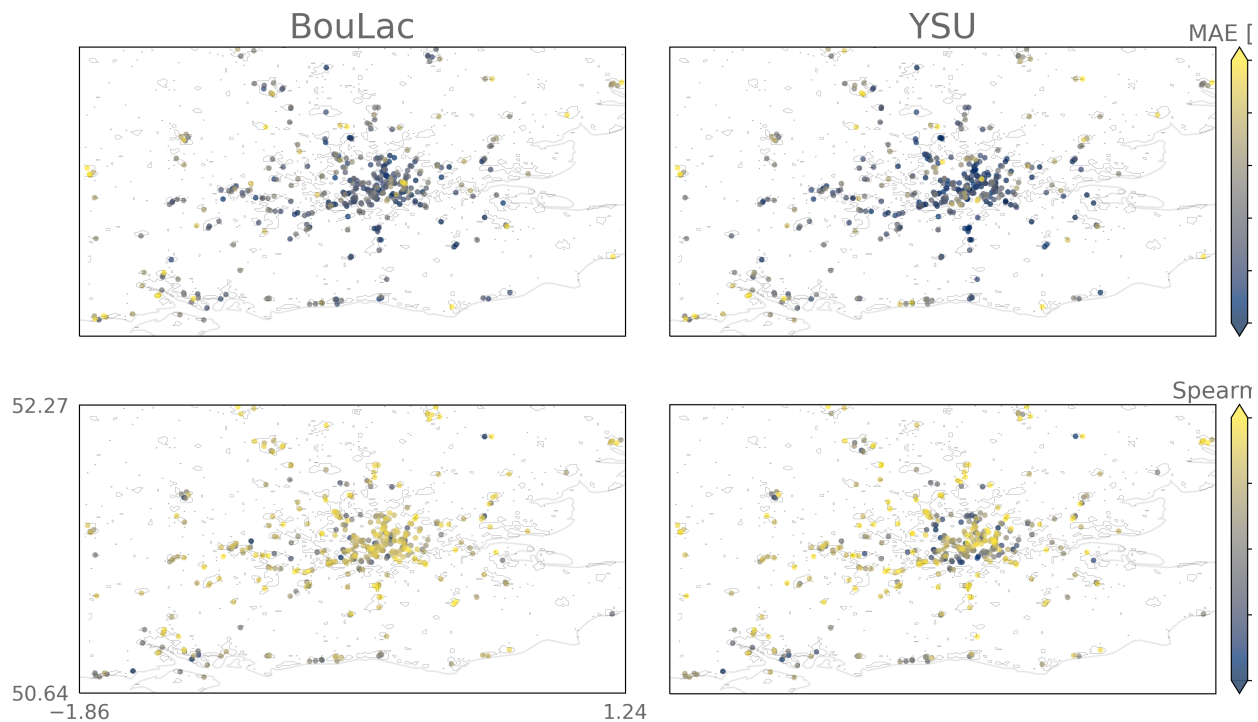


FIG. C1. Same as figure 3, but for MAE and Spearman's r.

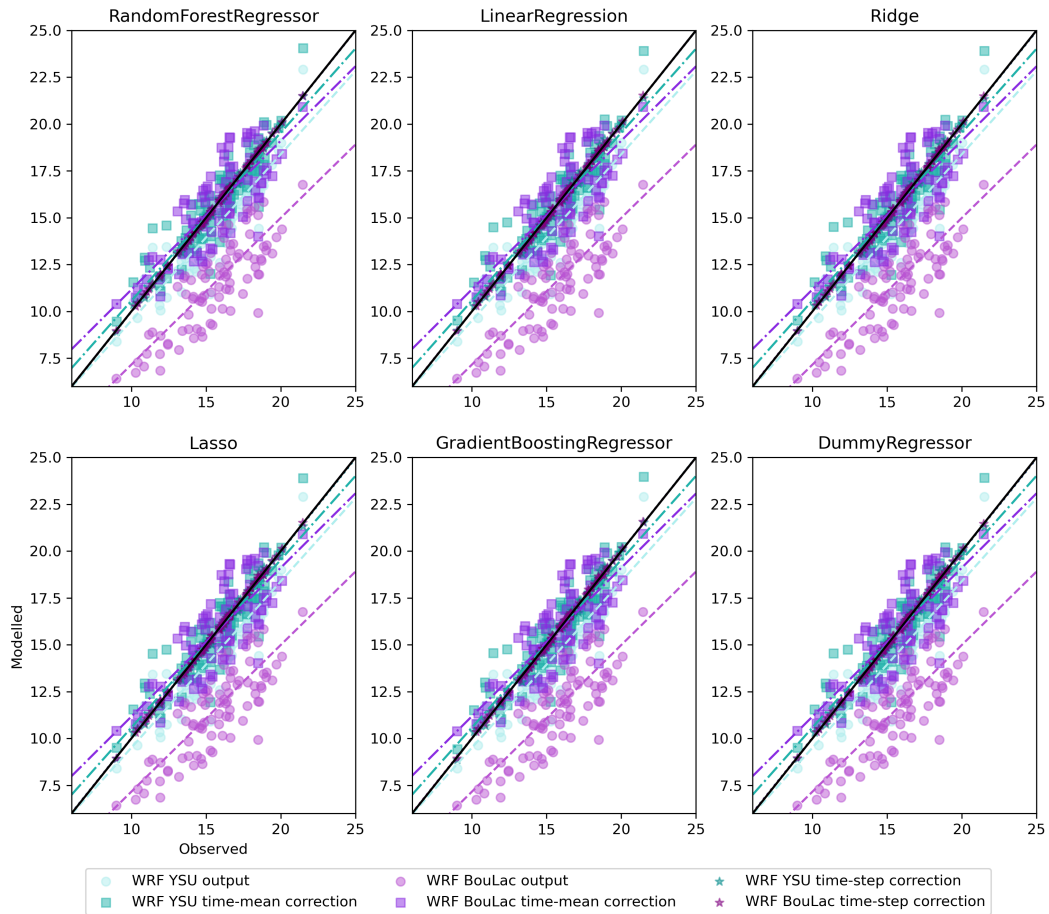
610 TABLE C1. Performance metrics used in Figure 4 for the model using Boulac prior to the bias-correction (WRF) and all the different regressors
611 (random forest: RF; linear regression: LR; Ridge regression: RD; Lasso regression: LA; gradient boosting: GB; and dummy regression: DU). The
612 different regressions are assigned a suffix: “avg” for regressions that were trained on the summer time-mean average of daily-minimum, -mean or
613 -maximum temperatures, and “step” for those that were trained with the temperatures at each daily time-step.

Boulac													
	WRF	RF_{avg}	RF_{step}	LR_{avg}	LR_{step}	RD_{avg}	RD_{step}	LA_{avg}	LA_{step}	GB_{avg}	GB_{step}	DU_{avg}	DU_{step}
MEAN													
RMSE	1.54	0.95	1.04	0.94	1.03	0.94	1.03	0.95	1.04	1.01	1.04	0.96	1.04
MAE	1.34	0.69	0.75	0.69	0.75	0.68	0.75	0.69	0.75	0.74	0.75	0.7	0.76
MB	-1.2	0.01	0.23	0	0.23	0	0.23	0	0.23	0	0.23	0.01	0.23
Pearson r²	0.11	0.09	0.07	0.09	0.07	0.1	0.07	0.1	0.07	0.06	0.06	0.11	0.08
Spearman r	0.37	0.33	0.32	0.33	0.31	0.36	0.32	0.36	0.32	0.29	0.32	0.37	0.33 0.88
MIN													
RMSE	1.42	0.93	0.94	0.92	0.93	0.92	0.93	0.92	0.93	1.01	0.96	0.92	0.94
MAE	1.15	0.72	0.73	0.71	0.72	0.71	0.72	0.71	0.73	0.79	0.74	0.71	0.73
MB	-1.08	0.01	0.02	0	0.02	0	0.02	0	0.02	0.04	0.02	0	0.02
Pearson r²	0.18	0.15	0.16	0.15	0.16	0.16	0.16	0.16	0.16	0.1	0.15	0.17	0.17
Spearman r	0.46	0.42	0.43	0.43	0.42	0.44	0.43	0.44	0.43	0.34	0.41	0.46	0.44
MAX													
RMSE	1.78	1.6	1.81	1.58	1.8	1.57	1.8	1.59	1.8	1.65	1.82	1.6	1.82
MAE	1.48	1.24	1.33	1.22	1.32	1.22	1.31	1.23	1.32	1.28	1.35	1.24	1.33
MB	-0.79	0	0.52	0	0.52	0	0.53	0.01	0.52	0	0.51	0.01	0.53
Spearman r	0.08	0.07	0.02	0.08	0.02	0.09	0.02	0.08	0.02	0.05	0.01	0.08	0.03
Spearman r	0.29	0.26	0.16	0.29	0.16	0.3	0.19	0.27	0.19	0.23	0.14	0.28	0.2

614 TABLE C2. Performance metrics used in Figure 4 for the model using YSU prior to the bias-correction (WRF) and all the different regressors (random
615 forest: RF; linear regression: LR; Ridge regression: RD; Lasso regression: LA; gradient boosting: GB; and dummy regression: DU). The different
616 regressions are assigned a suffix: “avg” for regressions that were trained on the summer time-mean average of daily-minimum, -mean or -maximum
617 temperatures, and “tstep” for those that were trained with the temperatures at each daily time-step.

	YSU												
	WRF	RF _{avg}	RF _{tstep}	LR _{avg}	LR _{tstep}	RD _{avg}	RD _{tstep}	LA _{avg}	LA _{tstep}	GB _{avg}	GB _{tstep}	DU _{avg}	DU _{tstep}
MEAN													
RMSE	1.33	1.09	1.16	1.07	1.16	1.08	1.16	1.09	1.18	1.15	1.17	1.1	1.19
MAE	1.04	0.82	0.86	0.82	0.86	0.82	0.87	0.83	0.89	0.87	0.85	0.84	0.89
MB	-0.76	0	0.17	0	0.17	0	0.17	0.01	0.16	0.02	0.17	0.01	0.17
Pearson r²	0.09	0.07	0.07	0.07	0.07	0.08	0.07	0.08	0.07	0.05	0.07	0.09	0.07
Spearman r	0.32	0.28	0.3	0.28	0.29	0.3	0.29	0.29	0.28	0.25	0.3	0.32	0.3
MIN													
RMSE	1.58	1.05	1.06	1.04	1.06	1.05	1.07	1.06	1.09	1.12	1.09	1.06	1.09
MAE	1.27	0.83	0.83	0.81	0.82	0.82	0.83	0.82	0.84	0.88	0.84	0.83	0.84
MB	-1.17	0	-0.03	0	-0.03	0	-0.03	0	-0.03	0.04	-0.02	0	-0.03
Pearson r²	0.11	0.1	0.1	0.1	0.1	0.1	0.1	0.1	0.09	0.08	0.1	0.11	0.1
Spearman r	0.37	0.35	0.37	0.35	0.36	0.34	0.35	0.34	0.34	0.31	0.36	0.36	0.35
MAX													
RMSE	1.65	1.63	1.82	1.6	1.81	1.6	1.8	1.6	1.8	1.67	1.82	1.6	1.8
MAE	1.32	1.25	1.33	1.23	1.31	1.23	1.31	1.23	1.31	1.29	1.34	1.23	1.31
MB	-0.41	0	0.49	0	0.5	0	0.5	0.01	0.49	-0.01	0.49	0.01	0.5
Pearson r²	0.09	0.07	0.04	0.08	0.05	0.09	0.05	0.09	0.05	0.06	0.04	0.09	0.05
Spearman r	0.32	0.27	0.23	0.29	0.24	0.31	0.25	0.3	0.26	0.25	0.22	0.31	0.26

Average model's bias correction of daily min temperature after 25 bootstrap



618 FIG. C2. Average modelled daily minimum air temperature at 2 m against observed at citizens' personal weather
 619 stations locations show that all machine learning regressors perform a similar bias-correction on average. In blue,
 620 modelled temperatures at 2 m are from the model simulation that used the Yonsei University (YSU) planetary
 621 boundary layer scheme before the bias correction (circles), after the summer time-mean bias correction (squares)
 622 and after the daily time-step bias correction (stars). In purple, the same values are given for the simulation which
 623 used the Bougeault-Lacarrère (BouLac) scheme. Dashed lines represent the least squares polynomial fitted lines
 624 and the black full line represents the identity line.

Average model's bias correction of daily max temperature after 25 bootstrap

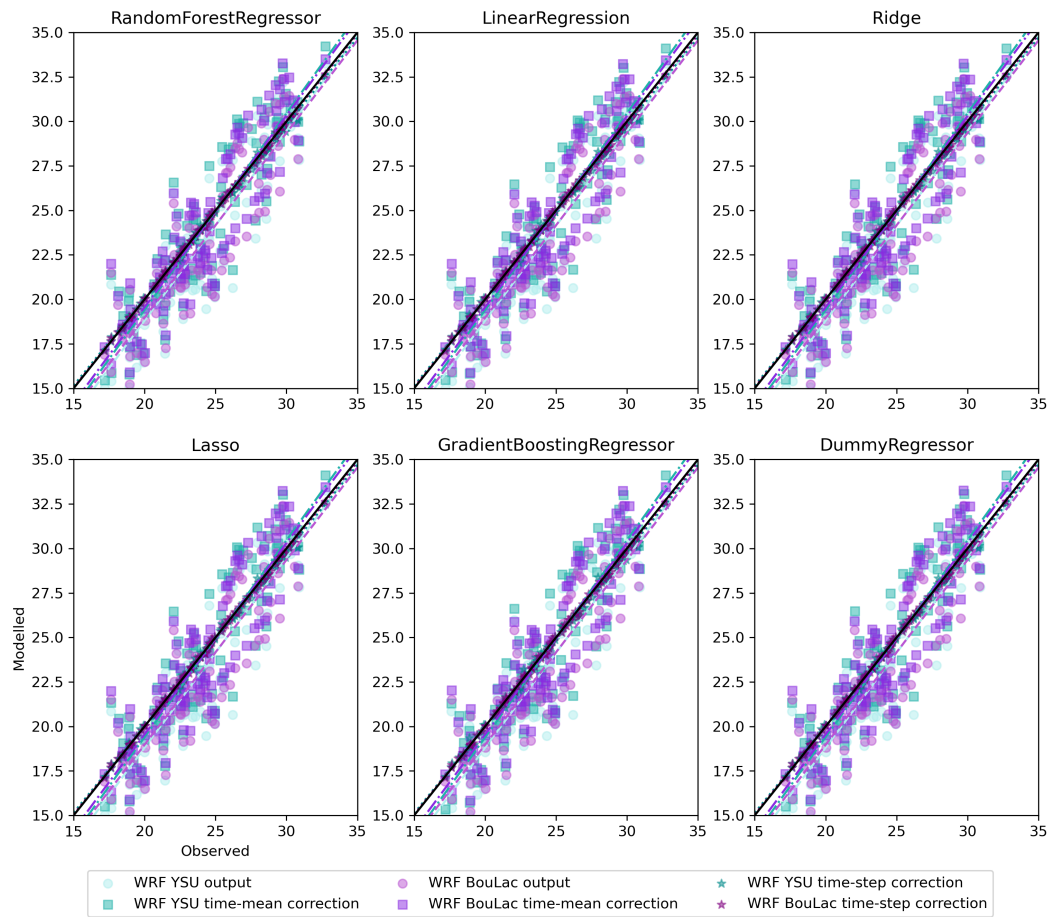


FIG. C3. Same as figure C2, but for daily maximum temperatures.

Average model's bias correction of daily mean temperature after 25 bootstrap

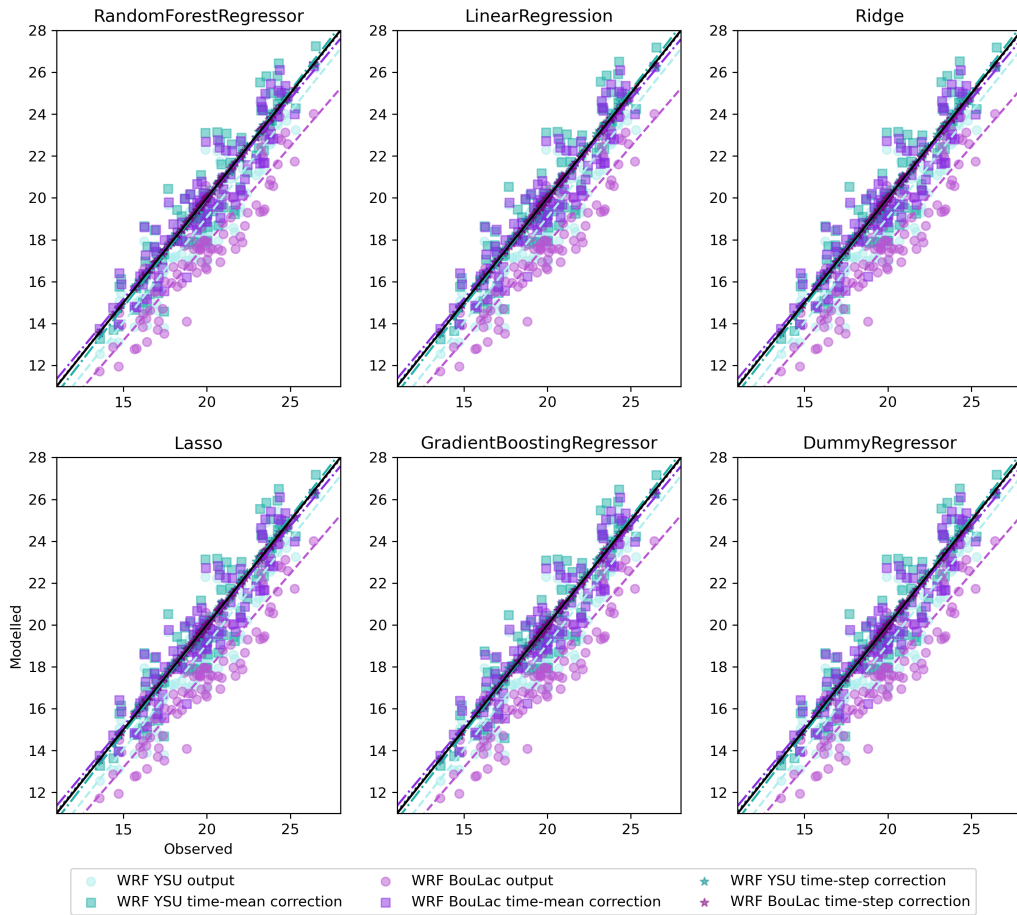


FIG. C4. Same as figure C2, but for daily mean temperatures.

Modelled temperatures and respective bias-corrections with multiple regressors

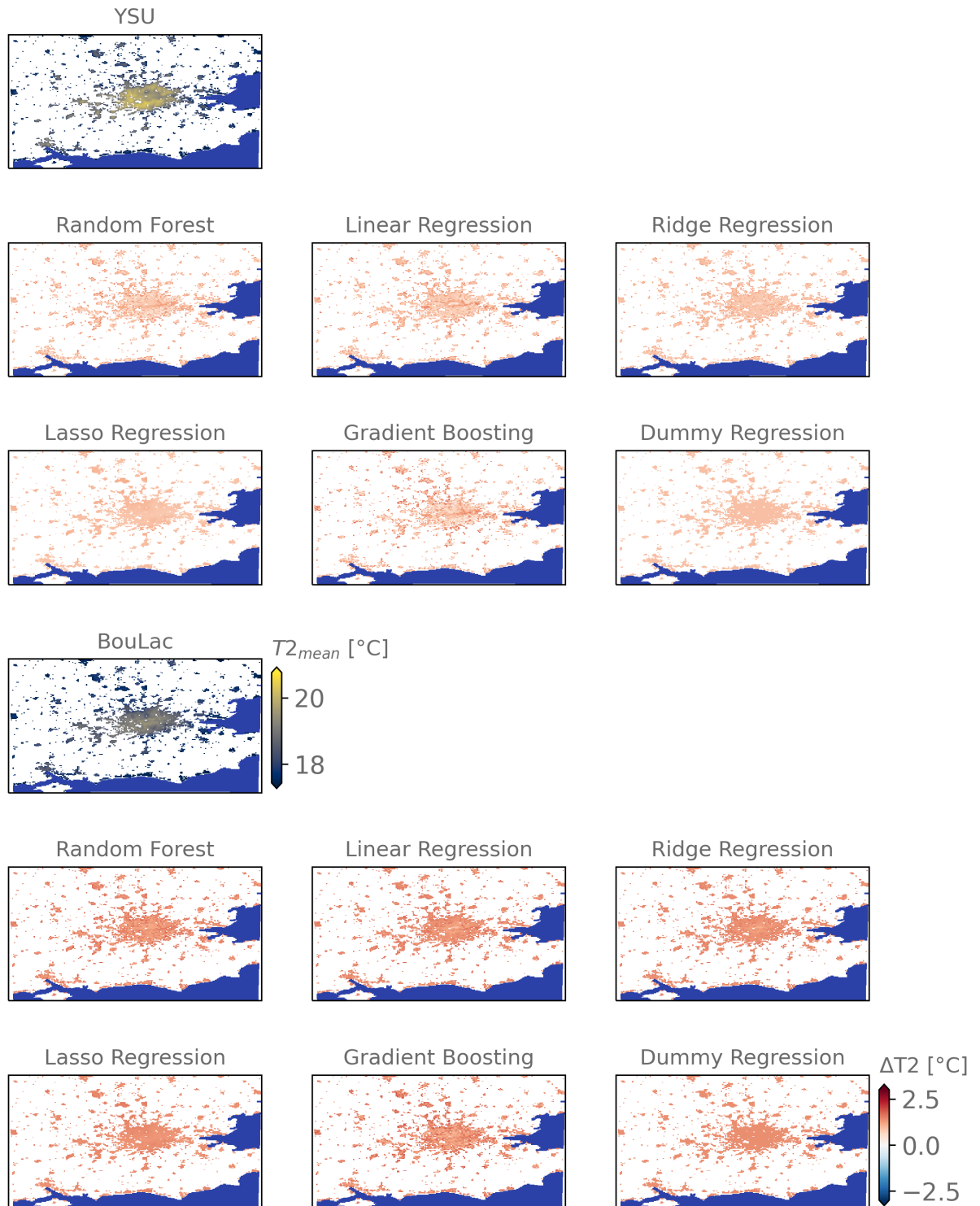


FIG. C5. Same as figure 5, but for daily mean temperatures.

Modelled temperatures and respective bias-corrections with multiple regressors

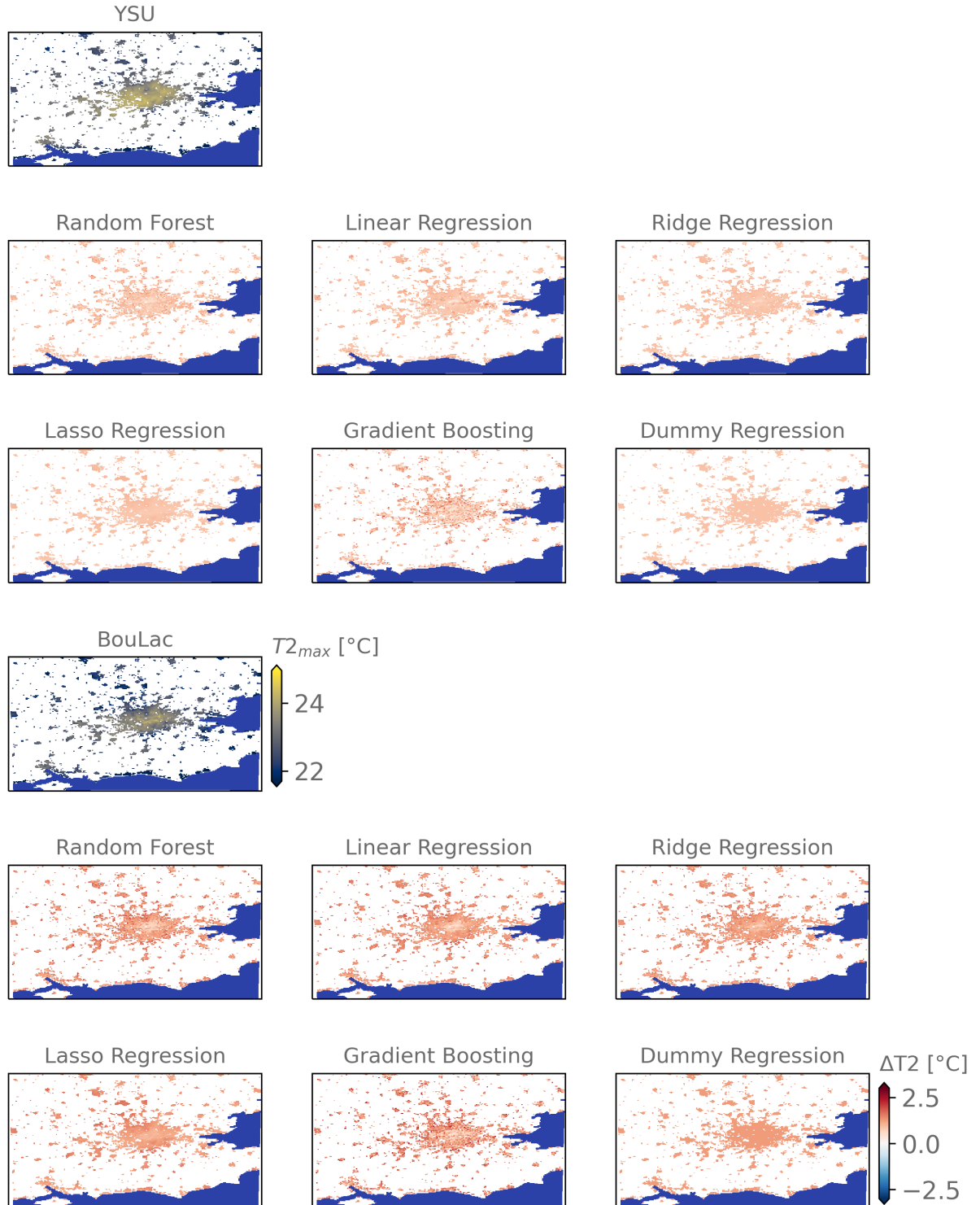


FIG. C6. Same as figure 5, but for daily maximum temperatures.

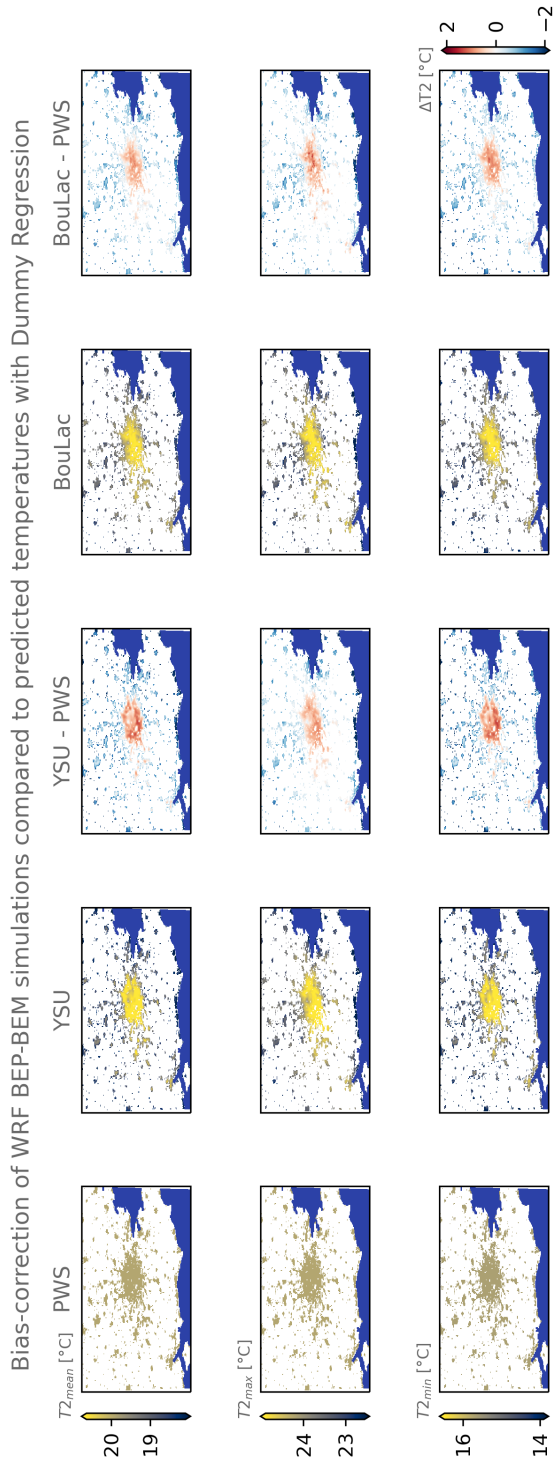


FIG. C7. Same as figure 6, but for dummy regression.

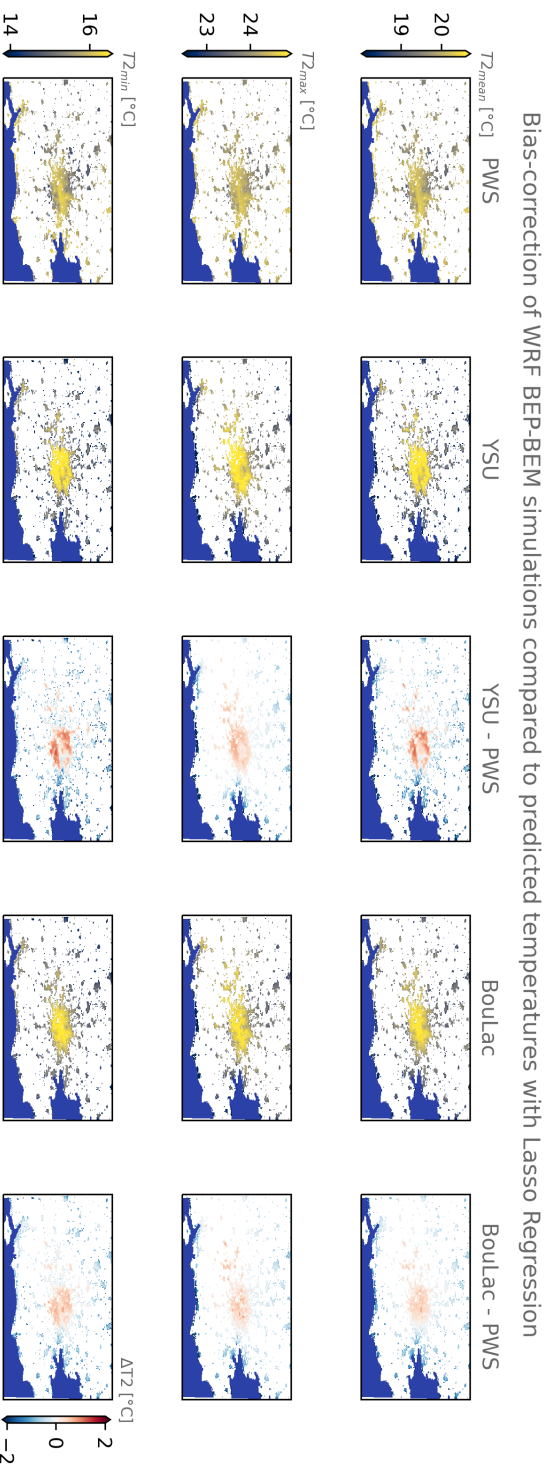


Fig. C8. Same as figure 6, but for Lasso regression.

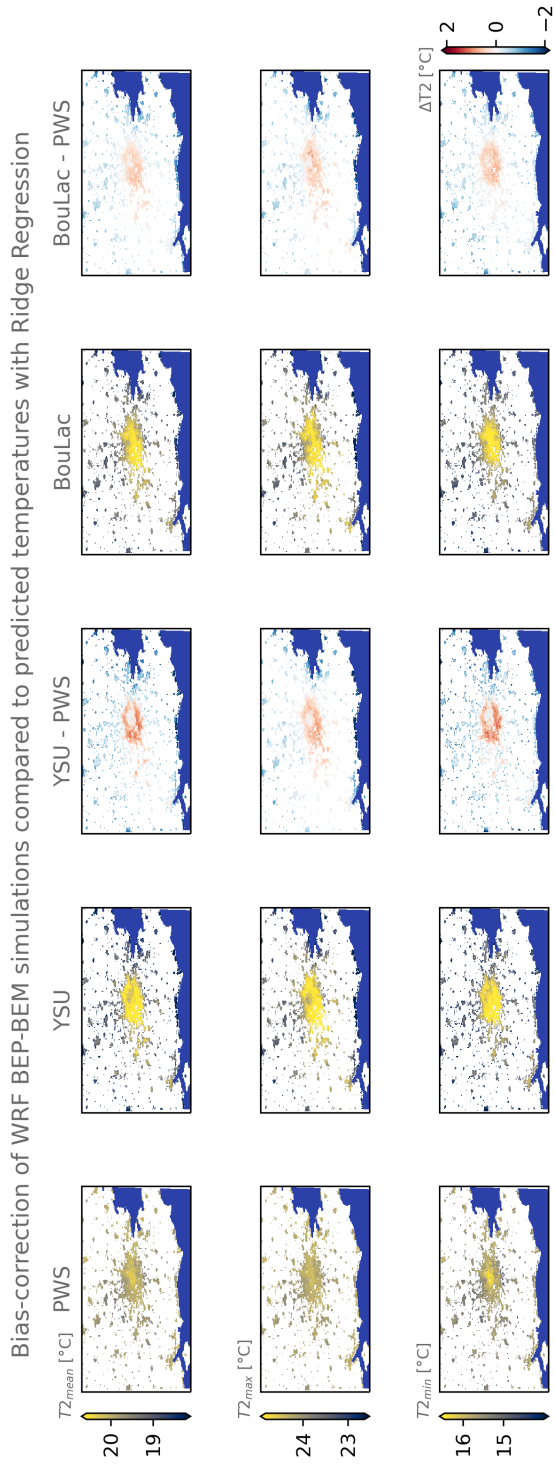


FIG. C9. Same as figure 6, but for Ridge regression.

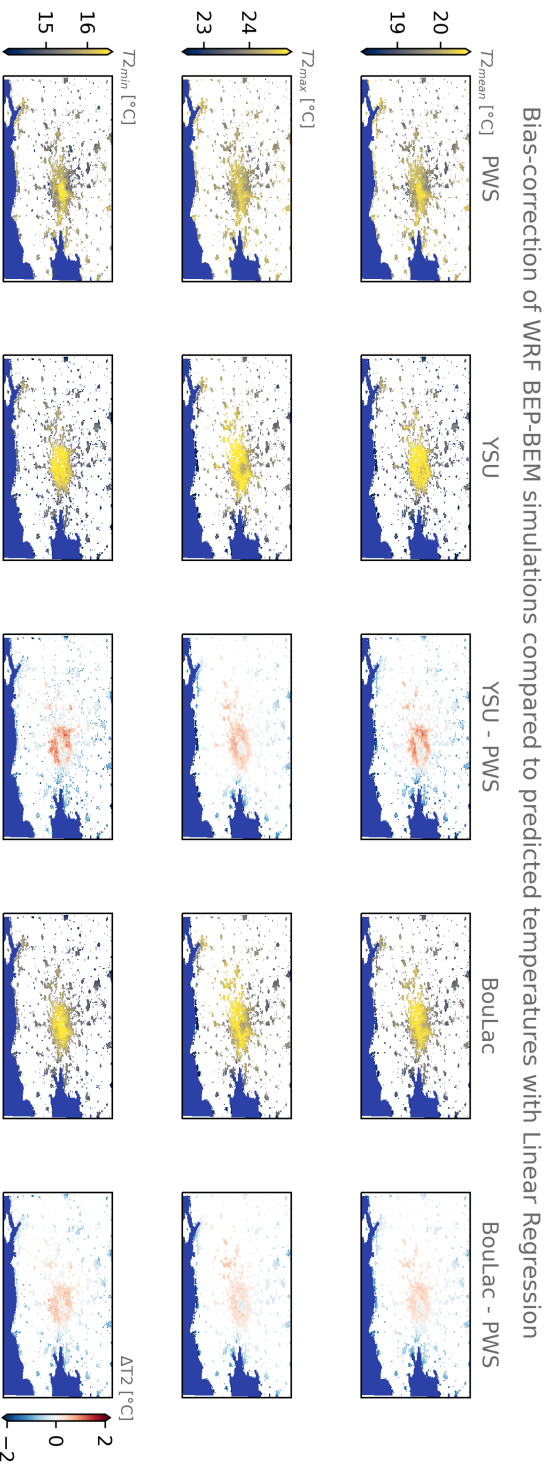


FIG. C10. Same as figure 6, but for linear regression.

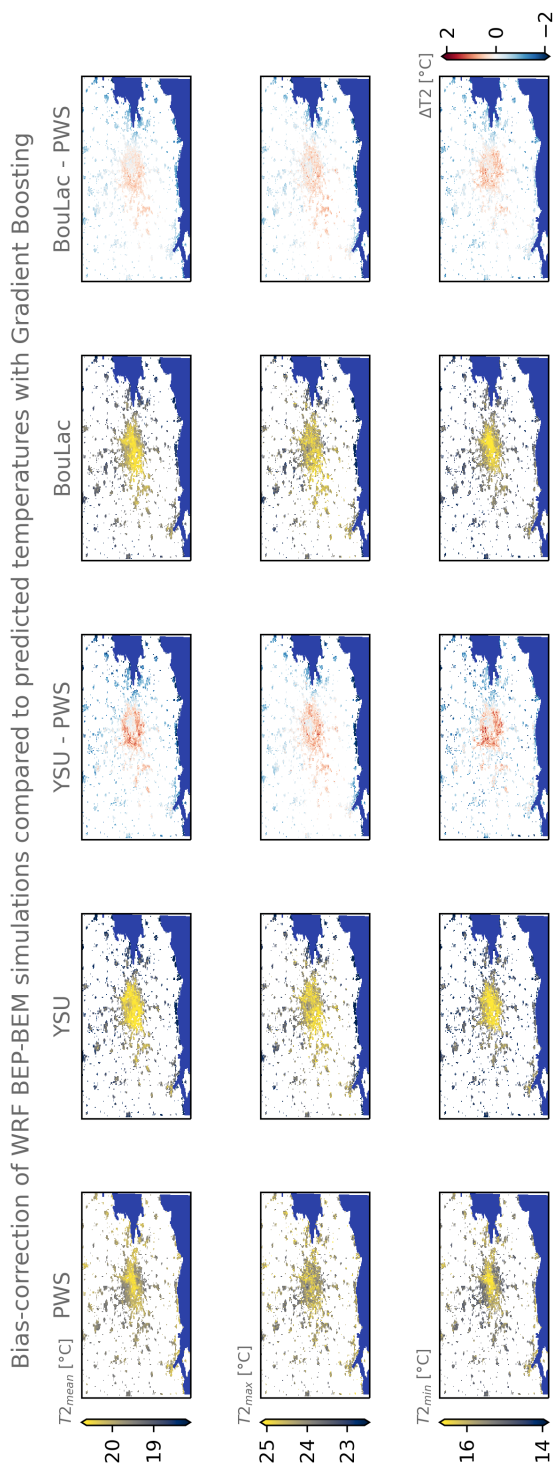


FIG. C11. Same as figure 6, but for gradient boosting regression.

625 **References**

- 626 Bassett, R., P. Young, G. Blair, F. Samreen, and W. Simm, 2020: A large ensemble approach to
627 quantifying internal model variability within the wrf numerical model. *Journal of Geophysical*
628 *Research: Atmospheres*, **125** (7), e2019JD031 286.
- 629 Benjamin, K., Z. Luo, and X. Wang, 2021: Crowdsourcing urban air temperature data for estimating
630 urban heat island and building heating/cooling load in london. *Energies*, **14** (16), 5208.
- 631 Bougeault, P., and P. Lacarrere, 1989: Parameterization of orography-induced turbulence in a
632 mesobeta–scale model. *Monthly weather review*, **117** (8), 1872–1890.
- 633 Brisson, E., M. Demuzere, and N. Van Lipzig, 2015: Modelling strategies for performing
634 convection-permitting climate simulations. *Meteorologische Zeitschrift*, **25** (2), 149–163.
- 635 Broadbent, A. M., J. Declet-Barreto, E. S. Krayenhoff, S. L. Harlan, and M. Georgescu, 2022:
636 Targeted implementation of cool roofs for equitable urban adaptation to extreme heat. *Science*
637 *of the Total Environment*, **811**, 151 326.
- 638 Brousse, O., A. Martilli, M. Foley, G. Mills, and B. Bechtel, 2016: Wudapt, an efficient land use
639 producing data tool for mesoscale models? integration of urban lcz in wrf over madrid. *Urban*
640 *Climate*, **17**, 116–134.
- 641 Brousse, O., C. Simpson, A. Poorthuis, and C. Heaviside, 2023: Unequal distributions of crowd-
642 sourced weather data in england and wales. Preprint available online, [https://doi.org/10.21203/](https://doi.org/10.21203/rs.3.rs-2715073/v1)
643 [rs.3.rs-2715073/v1](https://doi.org/10.21203/rs.3.rs-2715073/v1).
- 644 Brousse, O., C. Simpson, N. Walker, D. Fenner, F. Meier, J. Taylor, and C. Heaviside, 2022:
645 Evidence of horizontal urban heat advection in london using six years of data from a citizen
646 weather station network. *Environmental Research Letters*, **17** (4), 044 041.
- 647 Chapman, L., C. Bell, and S. Bell, 2017: Can the crowdsourcing data paradigm take atmospheric
648 science to a new level? a case study of the urban heat island of london quantified using netatmo
649 weather stations. *International Journal of Climatology*, **37** (9), 3597–3605.

650 Ching, J., and Coauthors, 2018: Wudapt: An urban weather, climate, and environmental modeling
651 infrastructure for the anthropocene. *Bulletin of the American Meteorological Society*, **99** (9),
652 1907–1924.

653 De Vos, L., A. Droste, M. Zander, A. Overeem, H. Leijnse, B. Heusinkveld, G. Steeneveld, and
654 R. Uijlenhoet, 2020: Hydrometeorological monitoring using opportunistic sensing networks
655 in the amsterdam metropolitan area. *Bulletin of the American Meteorological Society*, **101** (2),
656 E167–E185.

657 Demuzere, M., D. Argüeso, A. Zonato, and J. Kittner, 2021: W2w: A python package that
658 injects wudapt’s local climate zone information in wrf (version v0.1.1). Retrieved online, <https://pypi.org/project/w2w/>.
659

660 Demuzere, M., B. Bechtel, A. Middel, and G. Mills, 2019: Mapping europe into local climate
661 zones. *PloS one*, **14** (4), e0214474.

662 Demuzere, M., J. Kittner, A. Martilli, G. Mills, C. Moede, I. D. Stewart, J. van Vliet, and B. Bechtel,
663 2022: A global map of local climate zones to support earth system modelling and urban scale
664 environmental science. *Earth System Science Data Discussions*, 1–57.

665 Demuzere, M., and Coauthors, 2017: Impact of urban canopy models and external parameters on
666 the modelled urban energy balance in a tropical city. *Quarterly Journal of the Royal Meteorological Society*, **143** (704), 1581–1596.
667

668 Dudhia, J., 1989: Numerical study of convection observed during the winter monsoon experiment
669 using a mesoscale two-dimensional model. *Journal of Atmospheric Sciences*, **46** (20), 3077–
670 3107.

671 Fenner, D., B. Bechtel, M. Demuzere, J. Kittner, and F. Meier, 2021: Crowdqc+—a quality-control
672 for crowdsourced air-temperature observations enabling world-wide urban climate applications.
673 *Frontiers in Environmental Science*, 553.

674 Fenner, D., A. Holtmann, F. Meier, I. Langer, and D. Scherer, 2019: Contrasting changes of urban
675 heat island intensity during hot weather episodes. *Environmental Research Letters*, **14** (12),
676 124013.

677 Fenner, D., F. Meier, B. Bechtel, M. Otto, and D. Scherer, 2017: Intra and inter ‘local climate
678 zone’ variability of air temperature as observed by crowdsourced citizen weather stations in
679 berlin, germany. *10.14279/depositonce-10378*.

680 Georganos, S., and Coauthors, 2021: Geographical random forests: a spatial extension of the
681 random forest algorithm to address spatial heterogeneity in remote sensing and population
682 modelling. *Geocarto International*, **36 (2)**, 121–136.

683 Grassmann, T., A. Napoly, F. Meier, and D. Fenner, 2018: Quality control for crowdsourced data
684 from cws.

685 Grimmond, C. S. B., and Coauthors, 2011: Initial results from phase 2 of the international urban
686 energy balance model comparison. *International Journal of Climatology*, **31 (2)**, 244–272.

687 Gutiérrez, E., J. E. González, A. Martilli, R. Bornstein, and M. Arend, 2015: Simulations of a
688 heat-wave event in new york city using a multilayer urban parameterization. *Journal of Applied
689 Meteorology and Climatology*, **54 (2)**, 283–301.

690 Hammerberg, K., O. Brousse, A. Martilli, and A. Mahdavi, 2018: Implications of employing
691 detailed urban canopy parameters for mesoscale climate modelling: a comparison between
692 wudapt and gis databases over vienna, austria. *International Journal of Climatology*, **38**, e1241–
693 e1257.

694 Heaviside, C., X.-M. Cai, and S. Vardoulakis, 2015: The effects of horizontal advection on the
695 urban heat island in birmingham and the west midlands, united kingdom during a heatwave.
696 *Quarterly Journal of the Royal Meteorological Society*, **141 (689)**, 1429–1441.

697 Hendricks, E. A., J. C. Knievel, and Y. Wang, 2020: Addition of multilayer urban canopy models to
698 a nonlocal planetary boundary layer parameterization and evaluation using ideal and real cases.
699 *Journal of Applied Meteorology and Climatology*, **59 (8)**, 1369–1392.

700 Hollis, D., M. McCarthy, M. Kendon, T. Legg, and I. Simpson, 2019: Haduk-grid—a new uk
701 dataset of gridded climate observations. *Geoscience Data Journal*, **6 (2)**, 151–159.

702 Hong, S.-Y., J. Dudhia, and S.-H. Chen, 2004: A revised approach to ice microphysical processes
703 for the bulk parameterization of clouds and precipitation. *Monthly weather review*, **132 (1)**,
704 103–120.

- 705 Hong, S.-Y., and S.-W. Kim, 2008: Stable boundary layer mixing in a vertical diffusion scheme.
706 *18th Symposium on Boundary Layers and Turbulence B*, Vol. 16, 325.
- 707 Hong, S.-Y., Y. Noh, and J. Dudhia, 2006: A new vertical diffusion package with an explicit
708 treatment of entrainment processes. *Monthly weather review*, **134 (9)**, 2318–2341.
- 709 Janjić, Z. I., 2001: Nonsingular implementation of the mellor-yamada level 2.5 scheme in the ncep
710 meso model.
- 711 Janjić, Z. I., 1994: The step-mountain eta coordinate model: Further developments of the con-
712 vection, viscous sublayer, and turbulence closure schemes. *Monthly weather review*, **122 (5)**,
713 927–945.
- 714 Jiménez, P. A., J. Dudhia, J. F. González-Rouco, J. Navarro, J. P. Montávez, and E. García-
715 Bustamante, 2012: A revised scheme for the wrf surface layer formulation. *Monthly weather*
716 *review*, **140 (3)**, 898–918.
- 717 Kain, J. S., 2004: The kain–fritsch convective parameterization: an update. *Journal of applied*
718 *meteorology*, **43 (1)**, 170–181.
- 719 Lauwaet, D., H. Hooyberghs, B. Maiheu, W. Lefebvre, G. Driesen, S. Van Looy, and K. De Ridder,
720 2015: Detailed urban heat island projections for cities worldwide: dynamical downscaling
721 cmip5 global climate models. *Climate*, **3 (2)**, 391–415.
- 722 Lipson, M., S. Grimmond, and M. Best, 2021: Urban-plumber model evaluation project: initial
723 results. *EGU General Assembly Conference Abstracts*, EGU21–15 230.
- 724 Loridan, T., and C. Grimmond, 2012: Multi-site evaluation of an urban land-surface model: Intra-
725 urban heterogeneity, seasonality and parameter complexity requirements. *Quarterly Journal of*
726 *the Royal Meteorological Society*, **138 (665)**, 1094–1113.
- 727 Maraun, D., and M. Widmann, 2018: *Statistical downscaling and bias correction for climate*
728 *research*. Cambridge University Press.
- 729 Martilli, A., A. Clappier, and M. W. Rotach, 2002: An urban surface exchange parameterisation
730 for mesoscale models. *Boundary-layer meteorology*, **104 (2)**, 261–304.

- 731 Martilli, A., and Coauthors, 2021: Simulating the meteorology during persistent wintertime
732 thermal inversions over urban areas. the case of madrid. *Atmospheric Research*, **263**, 105–119.
- 733 Masson, V., 2000: A physically-based scheme for the urban energy budget in atmospheric models.
734 *Boundary-layer meteorology*, **94** (3), 357–397.
- 735 McCarthy, M., and Coauthors, 2019: Drivers of the uk summer heatwave of 2018. *Weather*, **74** (11),
736 390–396.
- 737 Meier, F., D. Fenner, T. Grassmann, M. Otto, and D. Scherer, 2017: Crowdsourcing air temperature
738 from citizen weather stations for urban climate research. *Urban Climate*, **19**, 170–191.
- 739 Mlawer, E. J., S. J. Taubman, P. D. Brown, M. J. Iacono, and S. A. Clough, 1997: Radiative transfer
740 for inhomogeneous atmospheres: Rrtm, a validated correlated-k model for the longwave. *Journal*
741 *of Geophysical Research: Atmospheres*, **102** (D14), 16 663–16 682.
- 742 Mughal, M. O., X.-X. Li, T. Yin, A. Martilli, O. Brousse, M. A. Dissegna, and L. K. Norford,
743 2019: High-resolution, multilayer modeling of singapore’s urban climate incorporating local
744 climate zones. *Journal of Geophysical Research: Atmospheres*, **124** (14), 7764–7785.
- 745 Muller, C., L. Chapman, S. Johnston, C. Kidd, S. Illingworth, G. Foody, A. Overeem, and R. Leigh,
746 2015: Crowdsourcing for climate and atmospheric sciences: current status and future potential.
747 *International Journal of Climatology*, **35** (11), 3185–3203.
- 748 Napoly, A., T. Grassmann, F. Meier, and D. Fenner, 2018: Development and application of a
749 statistically-based quality control for crowdsourced air temperature data. *Frontiers in Earth*
750 *Science*, **6**, 118.
- 751 Nazarian, N., and Coauthors, 2022: Integrated assessment of urban overheating impacts on human
752 life. *Earth’s Future*.
- 753 Niu, G.-Y., and Coauthors, 2011: The community noah land surface model with multiparameteri-
754 zation options (noah-mp): 1. model description and evaluation with local-scale measurements.
755 *Journal of Geophysical Research: Atmospheres*, **116** (D12).
- 756 Oke, T. R., G. Mills, A. Christen, and J. A. Voogt, 2017: *Urban climates*. Cambridge University
757 Press.

- 758 Oleson, K., G. Anderson, B. Jones, S. McGinnis, and B. Sanderson, 2018: Avoided climate impacts
759 of urban and rural heat and cold waves over the us using large climate model ensembles for rcp8.
760 5 and rcp4. 5. *Climatic change*, **146 (3)**, 377–392.
- 761 Pedregosa, F., and Coauthors, 2011: Scikit-learn: Machine learning in python. *the Journal of*
762 *machine Learning research*, **12**, 2825–2830.
- 763 Potgieter, J., N. Nazarian, M. J. Lipson, M. A. Hart, G. Ulpiani, W. Morrison, and K. Benjamin,
764 2021: Combining high-resolution land use data with crowdsourced air temperature to investigate
765 intra-urban microclimate. *Frontiers in Environmental Science*, 385.
- 766 Salamanca, F., A. Krpo, A. Martilli, and A. Clappier, 2010: A new building energy model coupled
767 with an urban canopy parameterization for urban climate simulations—part i. formulation,
768 verification, and sensitivity analysis of the model. *Theoretical and applied climatology*, **99 (3)**,
769 331–344.
- 770 Salamanca, F., and A. Martilli, 2010: A new building energy model coupled with an urban canopy
771 parameterization for urban climate simulations—part ii. validation with one dimension off-line
772 simulations. *Theoretical and Applied Climatology*, **99 (3)**, 345–356.
- 773 Salamanca, F., A. Martilli, M. Tewari, and F. Chen, 2011: A study of the urban boundary layer
774 using different urban parameterizations and high-resolution urban canopy parameters with wrf.
775 *Journal of Applied Meteorology and Climatology*, **50 (5)**, 1107–1128.
- 776 Salamanca, F., A. Martilli, and C. Yagiie, 2012: A numerical study of the urban heat island over
777 madrid during the desirex (2008) campaign with wrf and an evaluation of simple mitigation
778 strategies. *International Journal of Climatology*, **32 (15)**, 2372–2386.
- 779 Sgoff, C., W. Acevedo, Z. Paschalidi, S. Ulbrich, E. Bauernschubert, T. Kratzsch, and R. Pothast,
780 2022: Assimilation of crowd-sourced surface observations over germany in a regional weather
781 prediction system. *Quarterly Journal of the Royal Meteorological Society*.
- 782 Stewart, I. D., T. R. Oke, and E. S. Krayenhoff, 2014: Evaluation of the ‘local climate zone’ scheme
783 using temperature observations and model simulations. *International journal of climatology*,
784 **34 (4)**, 1062–1080.

- 785 Sunter, M., 2021: Midas data user guide for uk land observations, v20210705.
- 786 Tewari, M., F. Salamanca, A. Martilli, L. Treinish, and A. Mahalov, 2017: Impacts of projected
787 urban expansion and global warming on cooling energy demand over a semiarid region. *Atmo-
788 spheric Science Letters*, **18** (11), 419–426.
- 789 UKMO, 2021: Midas open: Uk hourly weather observation data, v202107. centre for envi-
790 ronmental data analysis, 08 september 2021. Data retrieved online, [https://doi.org/10.5285/
791 3bd7221d4844435dad2fa030f26ab5fd](https://doi.org/10.5285/3bd7221d4844435dad2fa030f26ab5fd).
- 792 Varentsov, M., D. Fenner, F. Meier, T. Samsonov, and M. Demuzere, 2021: Quantifying local
793 and mesoscale drivers of the urban heat island of moscow with reference and crowdsourced
794 observations. *Frontiers in Environmental Science*, 543.
- 795 Venter, Z. S., O. Brousse, I. Esau, and F. Meier, 2020: Hyperlocal mapping of urban air temperature
796 using remote sensing and crowdsourced weather data. *Remote Sensing of Environment*, **242**,
797 111 791.
- 798 Venter, Z. S., T. Chakraborty, and X. Lee, 2021: Crowdsourced air temperatures contrast satellite
799 measures of the urban heat island and its mechanisms. *Science Advances*, **7** (22), eabb9569.
- 800 Virtanen, P., and Coauthors, 2020: Scipy 1.0: fundamental algorithms for scientific computing in
801 python. *Nature methods*, **17** (3), 261–272.
- 802 Wang, J., and X.-M. Hu, 2021: Evaluating the performance of wrf urban schemes and pbl schemes
803 over dallas–fort worth during a dry summer and a wet summer. *Journal of Applied Meteorology
804 and Climatology*, **60** (6), 779–798.
- 805 Wouters, H., M. Demuzere, U. Blahak, K. Fortuniak, B. Maiheu, J. Camps, D. Tielemans, and
806 N. P. van Lipzig, 2016: The efficient urban canopy dependency parametrization (sury) v1. 0 for
807 atmospheric modelling: description and application with the cosmo-clm model for a belgian
808 summer. *Geoscientific Model Development*, **9** (9), 3027–3054.
- 809 Wouters, H., and Coauthors, 2017: Heat stress increase under climate change twice as large in
810 cities as in rural areas: A study for a densely populated midlatitude maritime region. *Geophysical
811 Research Letters*, **44** (17), 8997–9007.

- 812 Yang, J., and E. Bou-Zeid, 2019: Scale dependence of the benefits and efficiency of green and cool
813 roofs. *Landscape and urban planning*, **185**, 127–140.
- 814 Yang, Z.-L., and Coauthors, 2011: The community noah land surface model with multiparam-
815 eterization options (noah-mp): 2. evaluation over global river basins. *Journal of Geophysical*
816 *Research: Atmospheres*, **116 (D12)**.
- 817 Zängl, G., D. Reinert, P. Rípodas, and M. Baldauf, 2015: The icon (icosahedral non-hydrostatic)
818 modelling framework of dwd and mpi-m: Description of the non-hydrostatic dynamical core.
819 *Quarterly Journal of the Royal Meteorological Society*, **141 (687)**, 563–579.
- 820 Zonato, A., A. Martilli, S. Di Sabatino, D. Zardi, and L. Giovannini, 2020: Evaluating the
821 performance of a novel wudapt averaging technique to define urban morphology with mesoscale
822 models. *Urban Climate*, **31**, 100 584.
- 823 Zonato, A., A. Martilli, P. A. Jimenez, J. Dudhia, D. Zardi, and L. Giovannini, 2022: A new $k-\epsilon$
824 turbulence parameterization for mesoscale meteorological models. *Monthly Weather Review*.
- 825 Zumwald, M., B. Knüsel, D. N. Bresch, and R. Knutti, 2021: Mapping urban temperature using
826 crowd-sensing data and machine learning. *Urban Climate*, **35**, 100 739.